

Chiral analysis of the nucleon mass and sigma commutator

S. Owa,¹ D. B. Leinweber,² A. W. Thomas,¹ and X. G. Wang¹

¹*CSSM and ARC Centre of Excellence for Dark Matter Particle Physics,
Department of Physics, University of Adelaide, South Australia 5005, Australia*

²*CSSM, Department of Physics, University of Adelaide, South Australia 5005, Australia*

(Dated: June 28, 2024)

Schemes for describing the light quark mass dependence of the nucleon mass calculated in lattice QCD are compared. The three schemes in consideration include a fully relativistic and Lorentz covariant scheme, one that is fully relativistic but not Lorentz covariant, and a semirelativistic scheme utilizing the heavy baryon approximation. Calculations of observables involving pseudoscalar meson loop diagrams generate nonanalytic terms proportional to square roots and logarithms of the quark mass. The three schemes all yield the correct model independent leading and next-to-leading nonanalytic terms of the chiral expansion of the baryon mass. Results for the masses of the other members of the octet are also presented. Here, low-energy coefficients of the analytic terms of the expansion for the nucleon and hyperons are constrained by lattice QCD results and are demonstrated to be independent of the renormalization scheme used. The differences in the leading coefficient of the chiral expansions are found to be consistent with strange quark counting. Using the schemes examined herein, we report results for the pion-nucleon sigma commutator based upon recent lattice results from the CLS Collaboration. We find $\sigma_{\pi N} = 51.7 \pm 3.2 \pm 1.4$ MeV where the uncertainties are statistical and systematic respectively.

I. INTRODUCTION

The existence of lattice QCD calculations as a function of light quark mass offers important opportunities for gaining insight into hadron structure. There have been many studies of the dependence of nucleon properties on the masses of the light quarks, from its mass [1–22] to its electromagnetic [23–32] and axial form factors [33–37], the properties of its excited states [38–66], and most recently its generalized parton distributions [67–70]. Here we focus on the nucleon mass, and we report results for the other members of the octet. We also present a new result for the pion-nucleon light quark sigma commutator, $\sigma_{\pi N}$, based upon an analysis of the most recent CLS data [2].

In studying the nucleon mass, M_N , as a function of quark mass, chiral symmetry provides important guidance. First, we know that at leading order $m_N^2 \propto m_q$, where this appears to be a good approximation for values of m_π as large as 0.8 GeV. For this reason, we will show baryon masses as functions of m_π^2 . Second, terms involving odd powers of m_π or $\ln m_\pi$ are nonanalytic in the quark mass, with the leading and next-to-leading nonanalytic terms (LNA and NLNA) being proportional to m_π^3 and $m_\pi^4 \ln m_\pi$, respectively. These terms arise from pion loops and have coefficients which are, in principle, model independent.

Unfortunately, the convergence properties of an expansion of M_N in powers of m_π^2 plus the nonanalytic terms are poor. Indeed, the series is badly divergent outside the so called power counting regime (PCR), which corresponds roughly to m_π below 0.2 to 0.3 GeV. Attempts to fit lattice QCD results over a wider range of m_π have often led to values of the coefficients of the nonanalytic terms being adjusted to values which are inconsistent with the model independent constraints of chiral sym-

metry.

Here we have two key aims. First, we examine attempts to describe the nucleon mass from lattice QCD over a wide range of pion mass beyond the PCR. Of particular interest is an examination of relativistic effects in the effective field theory. We compare two relativistic formulations with the heavy baryon approximation to discern these effects. Finite-range regularization (FRR) is used to re-sum the power-series expansion and address larger pion masses in a careful manner, while preserving the leading and next-to-leading nonanalytic behavior of chiral perturbation theory exactly.

Three schemes are considered including a fully relativistic and Lorentz covariant scheme which uses a four-dimensional regulator; a fully relativistic scheme, similar to the covariant scheme, but using a three-dimensional regulator; and the semirelativistic heavy baryon (HB) approximation, corresponding to the limit of infinitely heavy baryons but including relativistic meson energies and using the three-dimensional regulator.

We find that the results obtained with these different schemes yield accurate and mutually compatible renormalized residual series coefficients (RSCs) of the lower powers of m_π^2 . This is in contrast to claims in the literature [71].

Second, having established the efficacy of the various formulations considered, we use them to tackle the highly topical question of the pion-nucleon sigma commutator.

The structure of this paper is as follows. In Sec. II we outline the theoretical framework, including a discussion of the nonanalytic behavior required by chiral symmetry, as well as the finite-volume corrections to the lattice QCD results. The degree of compatibility of the various schemes considered is investigated in Sec. III over a large range of m_π^2 using data generated by the PACS-CS collaboration [1]. Results are also presented for the other

members of the nucleon octet. In Sec. IV we analyze the latest lattice QCD results from the CLS collaboration [2] and compare the extracted low-energy constants (LECs) with contemporary analyses. This naturally leads to a study of the pion-nucleon sigma commutator, $\sigma_{\pi N}$. In Sec. V and VI we summarize our key findings and make some concluding remarks.

II. THEORETICAL FRAMEWORK

A. Chiral effective field theory

We present a chiral perturbation theory (χ PT)-inspired model which gives the same leading and next-to-leading model-independent terms in the chiral expansion. The effective $SU(3)_L \times SU(3)_R$ chiral Lagrangian (density) is given by

$$\mathcal{L} = \mathcal{L}_\phi + \mathcal{L}_{\phi B} + \mathcal{L}_{\phi T} + \mathcal{L}_{\phi BT}, \quad (1)$$

where \mathcal{L} consists of the free meson Lagrangian \mathcal{L}_ϕ , meson-octet Lagrangian $\mathcal{L}_{\phi B}$, meson-decuplet Lagrangian $\mathcal{L}_{\phi T}$, and the meson-octet-decuplet Lagrangian $\mathcal{L}_{\phi BT}$. Explicitly, at leading order, they are [71–74]

$$\begin{aligned} \mathcal{L}_\phi &= \frac{f_\phi^2}{4} \text{Tr} [D_\mu U (D^\mu U)^\dagger] + \frac{f_\phi^2}{4} \text{Tr} [\chi U^\dagger + U \chi^\dagger], \\ \mathcal{L}_{\phi B} &= \text{Tr} [\bar{B} (i \not{D} - M_B) B] - \frac{D}{2} \text{Tr} [\bar{B} \gamma^\mu \gamma_5 \{u_\mu, B\}] \\ &\quad - \frac{F}{2} \text{Tr} [\bar{B} \gamma^\mu \gamma_5 [u_\mu, B]], \\ \mathcal{L}_{\phi T} &= (\bar{T}_\mu)^{ijk} (i \gamma^{\mu\nu\alpha} D_\alpha - M_T \gamma^{\mu\nu}) (T_\nu)^{ijk}, \\ \mathcal{L}_{\phi BT} &= -\frac{\mathcal{C}}{2} \left[\epsilon^{ijk} (\bar{T}_\mu)^{ilm} \Theta^{\mu\nu} (u_\nu)^{lj} (B)^{mk} + \text{H.c.} \right], \quad (2) \end{aligned}$$

where f_ϕ is the pseudoscalar decay constant, D and F are the meson-octet coupling constants, \mathcal{C} is the meson-octet-decuplet constant, and M_B and M_T are the octet and decuplet baryon masses respectively. In the numerical calculations we use the values $f_\phi = 93$ MeV, $D = 0.86$ and $F = 0.41$ leading to $g_A = D + F = 1.27$, and $\mathcal{C} = (6/5)g_A$. Additionally, we have used the definition, $\gamma^{\mu\nu} \equiv \frac{1}{2} [\gamma^\mu, \gamma^\nu] = -i\sigma^{\mu\nu}$ and $\gamma^{\mu\nu\alpha} \equiv \frac{1}{2} \{\gamma^{\mu\nu}, \gamma^\alpha\} = i\epsilon^{\mu\nu\alpha\beta} \gamma_\beta \gamma_5$.

We also include the next-to-leading order (NLO) terms, corresponding to the Lagrangian [75]

$$\begin{aligned} \mathcal{L}_{\phi B}^{(2)} &= b_0 \text{Tr}[\chi_+] \text{Tr}[\bar{B}B] + b_D \text{Tr}[\bar{B}\{\chi_+, B\}] \\ &\quad + b_F \text{Tr}[\bar{B}[\chi_+, B]] + \sum_{i=1}^8 b_i O_i^{(2)} + \dots, \quad (3) \end{aligned}$$

where b_i are the NLO LECs of χ PT. We refer the readers to Appendix A for explicit expressions of the fields and the covariant derivatives of the Lagrangian.

Relevant to the later sections, we also present the NLO Lagrangian in the $SU(2)$ limit [76–78]

$$\begin{aligned} \mathcal{L}_{\pi N}^{(2)} &= c_1 \text{Tr}[\chi_+] \bar{\Psi} \Psi \\ &\quad - \frac{c_2}{4M_N^2} \text{Tr}[u_\mu u_\nu] (\bar{\Psi} D^\mu D^\nu \Psi + \text{H.c.}) \\ &\quad + \frac{c_3}{2} \text{Tr}[u^\mu u_\mu] \bar{\Psi} \Psi + \dots \quad (4) \end{aligned}$$

Here, c_i are the $SU(2)$ dimension-two LECs, Ψ is the nucleon doublet, and u (equivalently U) becomes the 2×2 unimodular unitary matrix with only pions.

B. Chiral expansion using FRR

Our focus here is on the analysis of lattice QCD data over a wide range of m_π^2 . As the naive series expansion is badly divergent for m_π beyond 0.2 to 0.3 GeV, we explore the application of FRR, which aims to re-sum the series in a physically motivated way [4, 5].

Historically, the FRR approach has had a number of successes, such as the accurate prediction of the strange quark contribution to the magnetic moment [24] and charge radius [25] of the proton, some years before experimental measurements confirmed the predictions [79–81]. It also led to the prediction of the excess of \bar{d} over \bar{u} quarks in the proton a decade before experimental confirmation [82]. Here, we are particularly interested in examining the historical criticism of the use of the heavy baryon approximation in early analyses of lattice QCD results.

In the analysis of the mass of the baryon as a function of meson mass using FRR, the mass of a baryon, B , is written as

$$M_B = a_0 + \sum_{\phi, \mathcal{B}'} a_{2,\phi} m_\phi^2 + a_{4,\phi} m_\phi^4 + \Sigma_{BB'\phi} + \Sigma_{B\phi, \text{tad}}, \quad (5)$$

where \mathcal{B}' denotes intermediate octet and decuplet baryons, and $a_{i,\phi}$ are the unrenormalized RSCs, which after renormalization relate to the LECs of the χ PT expansion. Details of the renormalization procedure are presented later in this section.

The self-energy contributions, Σ , are defined to be the on-shell matrix elements of the transition operator $\hat{\Sigma}$, that is

$$\Sigma = \frac{1}{2} \sum_s \bar{u}(p, s) \hat{\Sigma} u(p, s), \quad (6)$$

where u is the Dirac spinor, normalized as $\bar{u}(p, s) u(p, s') = \delta_{ss'}$, and the sum is taken over the spin of the external baryon state.

Illustrated in Fig. 1, we consider all possible octet-octet-meson, octet-decuplet-meson, and tadpole transitions. Note that the first two diagrams are generated by the leading order Lagrangian, while the tadpole diagram is solely generated by the NLO Lagrangian. All

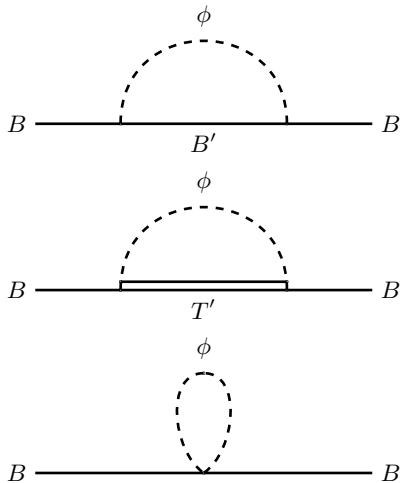


FIG. 1. Contributions to the octet baryon self-energies at $\mathcal{O}(p^4)$ from the χ EFT Lagrangian. These include octet-meson, decuplet-meson and tadpole terms. Note that there are additional diagrams that contribute to the tree-level correction at $\mathcal{O}(p^4)$ in χ PT, they are implicitly incorporated in our model through the series expansion of the baryon mass.

meson loops are included and the strange quark mass is fixed at its physical value. In this way, we do not expand about the SU(3) chiral limit, but rather the broken SU(3) limit, with $m_u = m_d$ (where m_u and m_d represent the light quark masses) and the strange quark mass fixed at its physical value. We refer to this as the light flavor chiral limit.

In principle, the computation of Eq. (5) is circular within the model, as M_B itself appears in the Lagrangian. This means that we require prior knowledge of M_B in the recursive calculation. At leading order approximation, one typically sets M_B to its physical value with no meson mass dependence. For a more sophisticated treatment, one could take some parametrization of M_B in terms of the pion mass from lattice QCD studies. In a preliminary analysis, we computed the renormalized RSCs for the nucleon and the pion-nucleon sigma commutator, and found that there is no significant difference between the results fixing M_N and using some parametrization of M_N . In light of this, we fix M_B in the Lagrangian density to their physical values for computational convenience.

The self-energy contributions from the relevant one-loop diagrams, for internal meson momentum k and external baryon momentum p , are

$$\hat{\Sigma}_{BB'\phi} = i \left(\frac{C_{BB'\phi}}{f_\phi} \right)^2 \int \frac{d^4 k}{(2\pi)^4} k \gamma_5 \frac{(\not{p} - \not{k} + M_B)}{D_{B'}} k \gamma_5 \frac{1}{D_\phi}, \quad (7)$$

$$\hat{\Sigma}_{BT'\phi} = i \left(\frac{C_{BT'\phi}}{f_\phi} \right)^2 \int \frac{d^4 k}{(2\pi)^4} \Theta^{\mu\nu} k_\nu \frac{(\not{p} - \not{k} + M_{T'}) \Lambda_{\mu\rho} (p - k)}{D_{T'}} \Theta^{\rho\sigma} k_\sigma \frac{1}{D_\phi}, \quad (8)$$

$$\hat{\Sigma}_{B\phi,\text{tad}} = i \frac{C_{B\phi,\text{tad}}}{f_\phi^2} \int \frac{d^4 k}{(2\pi)^4} \frac{1}{D_\phi}, \quad (9)$$

where $C_{BB'\phi}$ and $C_{B\phi,\text{tad}}$ are the octet-octet/decuplet-meson and octet-tadpole coupling constants, respectively (given in the Appendix B), $\Theta^{\mu\nu} = g^{\mu\nu} - \gamma^\mu \gamma^\nu$, the spin-3/2 projector is $\Lambda_{\mu\rho}(q) = g_{\mu\rho} - \frac{1}{3} \gamma_\mu \gamma_\rho - \frac{\gamma_\mu q_\rho - \gamma_\rho q_\mu}{3M_{T'}}$, and $D_X \equiv q^2 - m_X^2 + i\varepsilon$ with q and m_X being the momentum and mass of the hadron, respectively.

We commence with a consideration of a fully relativistic and Lorentz covariant formalism. In this case we introduce a 4-dimensional dipole form factor to regulate the divergent integrals

$$w(k) = \left(\frac{\Lambda^2}{k^2 - \Lambda^2} \right)^2, \quad (10)$$

where Λ is a cutoff scale. Correspondingly, in an alternate relativistic formalism (discussed in further detail in the next section) we use a 3-dimensional dipole regulator

$$w_{3D}(\vec{k}) = \left(\frac{\Lambda^2}{\vec{k}^2 + \Lambda^2} \right)^2. \quad (11)$$

This three-dimensional regulator is also used in the heavy baryon case. Closed expressions for the self-energies with these regulators are presented in Appendix C.

The essential feature of the FRR approach is that it guarantees the correct, model-independent, LNA and NLNA behavior of the nucleon mass as a function of m_π^2 . Of course, it also generates a nonanalytic term of order m_π^5 , which does depend on the regulator mass, Λ . However, the choice $\Lambda \in 0.8 - 1.0$ GeV, motivated by considerations of the size of the nucleon [3, 83–85] and analyses examining the renormalization flow of the LECs of the chiral expansion [13, 29, 86], is in reasonable agreement with the higher-order two-loop calculation of McGovern and Birse [87], which included an estimate of the effect of nucleon size on the nucleon self-energy within chiral perturbation theory.

The presence of multiple contact interactions in the formal expansion of the chiral Lagrangian density, in Eq. (3), with coefficients typically adjusted to describe pion-nucleon scattering [88] up to 70 MeV above thresh-

old, leads to tadpole diagrams which generate NLNA terms involving $m_\pi^4 \ln m_\pi$. In the limit where the pion mass is much less than $\Delta_{\Delta N}$ (the $\Delta - N$ mass difference), $m_\pi \ll \Delta_{\Delta N}$, the self-energy term $\Sigma_{N\Delta\pi}$ generates exactly this nonanalytic behavior. The coefficient of the NLNA term arising from $\Sigma_{N\Delta\pi}$ in this limit is approximately -3.1 GeV^{-1} , which lies within the range for the NLNA coefficient of the tadpole quoted by Frink and Meissner [89], namely $-8.4_{-4.4}^{+5.2} \text{ GeV}^{-1}$. However, in the physically more relevant case, where m_π is comparable to, or larger than Δ , the nonanalytic behavior involves a square root branch point at $m_\pi = \Delta$.

As the tadpole terms generated by the contact interactions will have overlap with a small- m_π expansion of the $\Delta\pi$ self-energy term, we examine the effect of including the explicit tadpole contribution of Eq. (9), with a coefficient in the range suggested in Ref. [89], but corrected for the $\Delta\pi$ contribution.

In any regularization scheme, the expressions of observables should preserve the symmetries of the underlying theory. Building from Ref. [90], it can be shown that the regulators presented above can be generated by an alternate chirally invariant Lagrangian. The alternate Lagrangian includes additional terms to the chiral effective theory (χEFT) Lagrangian, which modifies the hadron propagators to incorporate the regulator. Renormalization can be carried out using the extended on-mass-shell (EOMS) scheme [78], for which one systematically removes the chiral symmetry and power counting violating terms. While we do not strictly follow the EOMS renormalization, our renormalization scheme is tantamount to that of the EOMS scheme up to the desired order in the chiral expansion.

In this investigation, we make use of lattice QCD data to determine the renormalized RSCs of the chiral expansion. For the lattice data that we consider, the simulations are carried out in $N_f = 2 + 1$ flavours. Given that the strange quark mass is fixed (typically at the physical point), this serves as a good justification to consider the baryon mass expansion only in terms of the light quark mass expressed by m_π^2 . That is, using the Gell-Mann-Oakes-Renner relation with the strange quark mass fixed, at leading order, the squared kaon and eta masses can be written as a function of varying pion mass as

$$m_K^2 = \frac{1}{2}m_\pi^2 + \left(m_K^2|_{\text{phys}} - \frac{1}{2}m_\pi^2|_{\text{phys}} \right), \quad (12)$$

$$m_\eta^2 = \frac{1}{3}m_\pi^2 + \frac{4}{3} \left(m_K^2|_{\text{phys}} - \frac{1}{2}m_\pi^2|_{\text{phys}} \right), \quad (13)$$

where ‘‘phys’’ denotes the physical (experimental) value. As a result, the RSCs associated with each meson $a_{i,\phi}$ in Eq. (5) are absorbed into one a_i at each order of m_π^2 .

Given this background, we can now explicitly write the

renormalized chiral expansion of the baryon mass as

$$M_B = C_0^B + C_2^B m_\pi^2 + a_4^B m_\pi^4 + \sum_{\phi, B'} \left(\tilde{\Sigma}_{BB'\phi}(m_\pi^2) + \tilde{\Sigma}_{B\phi, \text{tad}}(m_\pi^2) \right), \quad (14)$$

where C_i^B are the renormalized RSCs unique to each baryon. Here, C_0^B is identified as the mass of the baryon in the light flavor chiral limit. The subtracted self-energies in Eq. (14) are defined by

$$\tilde{\Sigma}_{BB'\phi} \equiv \Sigma_{BB'\phi} - \Sigma_{BB'\phi}(0) - m_\pi^2 \frac{\partial \Sigma_{BB'\phi}}{\partial m_\pi^2}(0),$$

$$\tilde{\Sigma}_{B\phi, \text{tad}} \equiv \Sigma_{B\phi, \text{tad}} - \Sigma_{B\phi, \text{tad}}(0), \quad (15)$$

where, for brevity, $\Sigma(0) = \Sigma(m_\pi^2 = 0)$. The above is adequate in our renormalization scheme because the lowest order nonanalytic term starts at $\mathcal{O}(m_\pi^3)$ and the tadpole terms enter at $\mathcal{O}(m_\pi^4)$. For computational convenience we did not renormalize the coefficients of the terms analytic in m_q beyond $\mathcal{O}(m_\pi^2)$ (i.e., a_4 is left unrenormalized).

Evaluation of the NLNA contributions in our FR scheme reveals that the kaon contributions are small and vary slowly with changes in the pion mass. As a result we focus on the pion-loop contributions and consider the three SU(2) dimension-two LECs, c_1 , c_2 , and c_3 . These will be constrained by the requirement that our model respects the same nonanalytic behavior as SU(2) χPT up to and including $\mathcal{O}(m_\pi^4 \ln m_\pi)$ for the nucleon.

In order to estimate the tadpole contribution to the mass of the nucleon, we first consider the values of c_1 , c_2 , and c_3 , summarised in Refs. [9, 91], where these LECs were determined based on phenomenological considerations. Although they are determined from different schemes (where the associated higher-order terms differ), the physical pion mass is well within the PCR such that higher order terms do not contribute in a significant manner. The role of these LECs is to set a plausible central value for the nucleon-pion tadpole coefficient. Despite the rather expansive uncertainty range on the LECs from the aforementioned references, we extend this range by considering LECs more recently determined from Ref. [92]. We consider results with explicit Δ degrees of freedom because the LECs undergo significant changes with the explicit inclusion of Δ . Thus, with significant error bounds, we evaluate the effects of the tadpole term in the final result. Matching subtleties between SU(2) and SU(3) χPT are not considered.

In χPT , the nucleon-pion tadpole self-energy is written as [?]]

$$\Sigma_{N\pi, \text{tad}} = -i \frac{3}{f_\phi^2} \left(-2c_1 + \frac{c_2}{4} + c_3 \right) m_\pi^2 \int \frac{d^4 k}{(2\pi)^4} \frac{1}{D_\pi}. \quad (16)$$

In the relativistic theory, the $NN\pi$ self-energy contributes both a LNA contribution proportional to m_π^3 and a NLNA contribution proportional to $m_\pi^4 \ln m_\pi$, such that the coefficient of the NLNA term, k_3 , in the

χ PT nucleon mass expansion (discussed later in Sec. V A Eq. (28)) is

$$k_3 = -\frac{3}{32\pi^2 f_\phi^2} \left(-8c_1 + c_2 + 4c_3 + \frac{g_A^2}{M_N} \right). \quad (17)$$

It is precisely the combination of c_1 , c_2 , and c_3 in Eq. (16) minus the contribution from the $N\Delta\pi$ loop, discussed earlier, that we take as a single parameter χC as

$$\chi C \equiv -2c_1 + \frac{c_2}{4} + c_3 + \frac{\mathcal{A}}{4} = -1.3_{-1.1}^{+3.3} \text{ GeV}^{-1}, \quad (18)$$

from Refs. [9, 91] and upper bound appropriately extended to encapsulate values (with explicit Δ) from Ref. [92]. \mathcal{A} is proportional to the $N\Delta\pi$ NLNA contribution and is given by

$$\mathcal{A} \equiv \frac{24}{25} g_A^2 \frac{M_N^2}{\Delta_{\Delta N} (M_N + \Delta_{\Delta N})^2} \approx 3.1 \text{ GeV}^{-1}, \quad (19)$$

quoted earlier. The $\Delta - N$ mass difference, $\Delta_{\Delta N}$, is taken at the physical point. In this manner, k_3 in our model is congruent to that of χ PT, once we separately include the $N\Delta\pi$ self-energy contribution

$$k_3 = -\frac{3}{32\pi^2 f_\phi^2} \left(4\chi C - \mathcal{A} + \frac{g_A^2}{M_N} \right). \quad (20)$$

C. Finite-volume corrections

In order to fit the chiral expansion to lattice results, one either needs to compute the expansions in finite-volume, or to correct the lattice results to infinite-volume. For the latter case, it is necessary to calculate the finite-volume corrections (FVCs). Following common practice, we choose to treat the spatial and temporal dimensions differently, such that the temporal integral is performed over infinite-volume. Then, for some FRR integrand, $I(\vec{k}, m_\pi^2, \Lambda)$, the FVC is defined as follows

$$\delta^{\text{FVC}}(m_\pi^2, L, \Lambda) \equiv \int \frac{d^3 k}{(2\pi)^3} I(\vec{k}, m_\pi^2, \Lambda) - \frac{1}{L^3} \sum_{\vec{k}} I(\vec{k}, m_\pi^2, \Lambda), \quad (21)$$

where L is the length of the box. The lattice QCD results are corrected to infinite-volume through the addition of $\delta^{\text{FVC}}(m_\pi^2, L, \Lambda)$ to each finite-volume lattice value.

It has been demonstrated that in an earlier study of Ref. [13], FVCs of self-energy integrals, using the same regulator presented in Eq. (11), have negligible dependence on Λ beyond 0.8 GeV. At a box size of $L = 2.9$ fm, the FVCs vary by about 1 MeV in the domain $0.8 \leq \Lambda \leq 2.4$ GeV.

III. HEAVY BARYON VERSUS RELATIVISTIC FORMALISMS

A. The correspondence of the schemes

In order to compare the application of the HB approximation with relativistic approaches for analyzing lattice QCD data for $M_N(m_\pi^2)$, we consider three schemes:

1. Covariant (Cov) - a fully relativistic and Lorentz covariant scheme which uses the four-dimensional dipole regulator of Eq. (10),
2. Relativistic (Rel) - a fully relativistic scheme, similar to the covariant scheme, but uses the three-dimensional dipole regulator of Eq. (11), and
3. Heavy baryon (HB) - a semirelativistic scheme corresponding to the limit of infinitely heavy baryons but including relativistic meson energies and using the three-dimensional dipole regulator.

One may obtain the self-energy expressions in the HB scheme by performing the k_0 integral of Eqs. (7)-(9) and taking the limit M_B and $M_{B'}$ to infinity in the relativistic scheme. We obtain

$$\Sigma_{BB'\phi}^{(\text{HB})} = -\frac{1}{2} \left(\frac{C_{BB'\phi}}{f_\phi} \right)^2 \int \frac{d^3 k}{(2\pi)^3} \frac{k^2}{\omega_k(\omega_k + \delta)}, \quad (22)$$

$$\Sigma_{BT'\phi}^{(\text{HB})} = -\frac{1}{3} \left(\frac{C_{BT'\phi}}{f_\phi} \right)^2 \int \frac{d^3 k}{(2\pi)^3} \frac{k^2}{\omega_k(\omega_k + \Delta)}, \quad (23)$$

$$\Sigma_{B\phi, \text{tad}}^{(\text{HB})} = \frac{1}{2} \frac{C_{B\phi, \text{tad}}}{f_\phi^2} \int \frac{d^3 k}{(2\pi)^3} \frac{1}{\omega_k}, \quad (24)$$

where δ (Δ) is the mass difference between the external octet and the internal octet (decuplet) baryon. The meson energy is $\omega_k = \sqrt{k^2 + m_\phi^2}$.

As the regulator cutoff parameters, Λ , are *a priori* not the same in different schemes, we can determine a correspondence between the three cutoff scales $\Lambda_{(\text{Cov})}$, $\Lambda_{(\text{Rel})}$, and $\Lambda_{(\text{HB})}$. This correspondence allows for a reasonable comparison between the schemes, since it may compensate for the differences in the suppression of large momenta.

The correspondence between the cutoff scales is determined by computing the self-energy contributions in one scheme, and fitting the others to it. Given the abundance of literature pointing towards the optimal range $0.8 \leq \Lambda_{(\text{HB})} \leq 1.0$ GeV for the HB scheme in SU(2), we fix $\Lambda_{(\text{HB})} = 0.8$ GeV and perform a fit of the form

$$\sum_{\phi, B'} \tilde{\Sigma}_{BB'\phi}^{(\text{HB})}(m_\pi^2, \Lambda_{(\text{HB})}) \approx d_4^{(\text{Cov/Rel})} m_\pi^4 + \sum_{\phi, B'} \tilde{\Sigma}_{BB'\phi}^{(\text{Cov/Rel})}(m_\pi^2, \Lambda_{(\text{Cov/Rel})}), \quad (25)$$

over the domain $0.0 \leq m_\pi^2 \leq 0.6$ GeV², by adjusting d_4 and Λ .

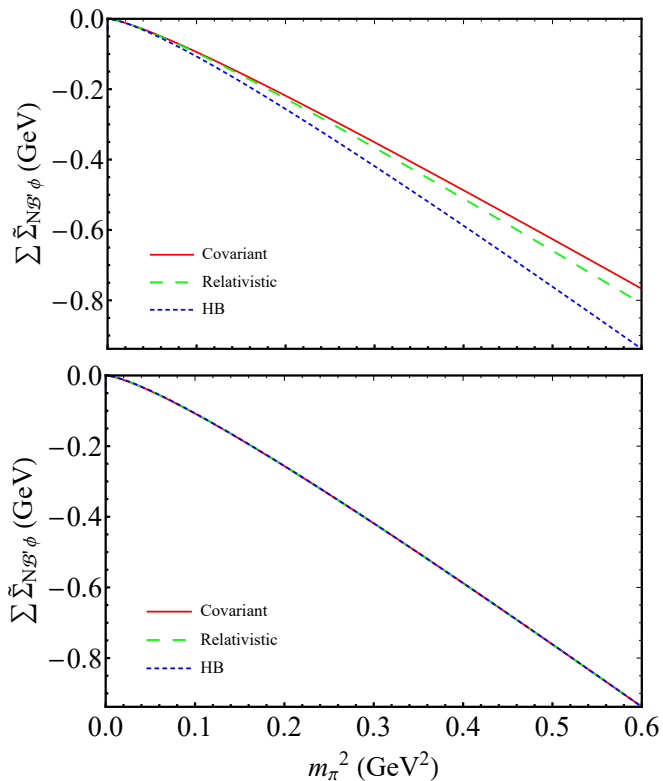


FIG. 2. Sum of all FRR renormalized nucleon-baryon-meson self-energy contributions in different schemes. The upper figure compares the schemes at the same cutoff scale $\Lambda_{(\text{Cov})} = \Lambda_{(\text{Rel})} = \Lambda_{(\text{HB})} = 0.8$ GeV. The bottom figure shows the fit of the relativistic schemes to the HB scheme at $\Lambda_{(\text{HB})} = 0.8$ GeV. The fit parameters are shown in Table I.

We note that the subtracted self-energies are void of the leading constant and m_π^2 terms. Since we left a_4 unrenormalized in Eq. (14), we have introduced the d_4 term to compensate for the differences at $\mathcal{O}(m_\pi^4)$. Such a difference will simply be absorbed by a_4 when performing the fits to lattice data.

In Fig. 2 we show the sum of all FRR renormalized nucleon-baryon-meson self-energy contributions for each

TABLE I. Regulator mass and difference in unrenormalized coefficient of m_π^4 determined by fitting the corresponding self-energies calculated in the HB scheme (Eq. (25)), using $\Lambda_{(\text{HB})} = 0.8$ GeV.

| Scheme | Baryon | Λ (GeV) | d_4 (10^{-2} GeV $^{-3}$) |
|--------------|---------|-----------------|---------------------------------|
| Covariant | Nucleon | 1.05 | 0.69 |
| | Lambda | 1.15 | 8.82 |
| | Sigma | 0.93 | -0.01 |
| | Xi | 1.04 | 2.74 |
| Relativistic | Nucleon | 1.01 | 6.78 |
| | Lambda | 1.06 | 9.79 |
| | Sigma | 0.91 | 2.38 |
| | Xi | 0.98 | 3.20 |

scheme. As we see in the top half, the relativistic schemes do differ at the 10-20% level when the same cutoff mass, 0.8 GeV, is used in all of them. However, as shown in the bottom half of Fig. 2, if we allow the values of the cutoff mass to vary with scheme, one finds excellent agreement between all three. The variation in Λ is indeed somewhat subtle. While not presented here, qualitatively, the plots for $\sum_{\phi, \mathcal{B}'} \tilde{\Sigma}_{\Lambda \mathcal{B}' \phi}$, $\sum_{\phi, \mathcal{B}'} \tilde{\Sigma}_{\Sigma \mathcal{B}' \phi}$, and $\sum_{\phi, \mathcal{B}'} \tilde{\Sigma}_{\Xi \mathcal{B}' \phi}$ as a function of m_π^2 are virtually the same to that of Fig. 2.

While we have considered one value of Λ for the sum over intermediate baryons in this comparison, one may conduct a comparison on a diagram-by-diagram basis. In such a case, one could theoretically have different regulator cutoffs for each baryon-baryon-meson contribution. This is because the regulator is associated with the induced pseudoscalar form factor of the baryon in phenomenological models. Lattice QCD calculations have demonstrated that strange quarks are more localized, which suggests that regulators, and thus the cutoff, might be expected to vary for each baryon, depending on the number of strange quarks present. However, with the level of agreement seen in Table I between the octet baryons and the schemes, it seems sufficient to adopt the standard approach and only have one regulator parameter. Therefore, we set $\Lambda_{(\text{Cov})} = \Lambda_{(\text{Rel})} = 1.0$ GeV in the subsequent fits.

B. Fit Strategy

The fitting procedure is as follows. Firstly, we apply the FVCs of Sec. IIC to the lattice results, taking them from finite to infinite-volume.

Then, we fit the infinite-volume results available at several quark masses and lattice spacings to a function containing both the physics of chiral nonanalytic behavior and a term linear in the square of the lattice spacing to address finite lattice spacing corrections at $\mathcal{O}(a^2)$. For the nucleon, we have

$$M_N = C_0 + C_2 m_\pi^2 + a_4 m_\pi^4 + \tilde{\Sigma}_{NN\pi} + \tilde{\Sigma}_{N\Lambda K} + \tilde{\Sigma}_{N\Sigma K} + \tilde{\Sigma}_{NN\eta} + \tilde{\Sigma}_{N\Delta\pi} + \tilde{\Sigma}_{N\Sigma^* K} + \tilde{\Sigma}_{N\pi, \text{tad}} + D_a a^2, \quad (26)$$

where, specifically for the nucleon, we have dropped the superscript N on the RSCs. We note the PACS-CS results are obtained with a nonperturbatively improved Wilson-Clover fermion action such that the leading lattice artifact is the same as for the CLS results [2], and addressed at $\mathcal{O}(a^2)$ by the final term in Eq. (26).

The fit parameters include C_0 , C_2 , a_4 and D_a . With the parameters constrained by lattice QCD results, one can then use Eq. (26) to interpolate/extrapolate to any value of m_π^2 or lattice spacing approaching the continuum limit. For example, one can expose the lattice spacing dependence of the lattice results by using Eq. (26) without the final term to access the physical quark masses and then plot the results as a function of a^2 .

As a final step, we also explore the addition of the physical baryon mass to the data set and refit to obtain our best estimates of the renormalized RSCs.

In order to check the degree of model dependence associated with the three schemes under consideration, we compare our renormalized RSCs, C_0 and C_2 to the linear combinations of SU(2) LECs reported using χ PT.

Finally, given the large uncertainty in the tadpole coefficient of Eq. (18), we consider the upper and lower bounds of this coefficient as a source of systematic uncertainty.

C. Fit to PACS-CS lattice QCD data

Recent advances in computational capabilities and techniques have led to lattice QCD calculations near physical values of the light quark masses. Our aim in this section is compare analyses of the historical PACS-CS lattice QCD results [1], which extend over a wide range of pion mass, using the three schemes described. Note that we choose to exclude two data points from the PACS-CS data set – one near the physical point with $m_\pi L \approx 2$, and one simulated with a different strange quark mass.

In the case of the PACS-CS data set [1], we cannot readily calculate the $\mathcal{O}(a^2)$ leading lattice artifact correction, because the lattice spacing is kept constant in the PACS-CS scheme. As an initial fit, we set $D_a = 0$ in Eq. (26). The results of this initial fit are shown in Fig. 3 and Table II.

We note that the uncertainty associated with the physical point is several orders of magnitude smaller than that of the lattice data, which means that the goodness of fit is primarily determined by the physical point. Therefore, to have some reasonable gauge of the goodness of fit, we exclude the physical point in the χ^2_{dof} calculation.

As seen in Fig. 3, the fits to the PACS-CS data are virtually indistinguishable. The χ^2_{dof} is approximately 0.26 for all three schemes. Not only are the fits to the data over values of $m_\pi^2 \in 0.02 - 0.50$ GeV² using the three schemes extremely close but, as we see in Table II, the renormalized RSCs C_0 and C_2 are also completely consistent. It is also necessary to examine if the value

TABLE II. Fits to the nucleon RSCs obtained from the PACS-CS nucleon mass lattice QCD results of Ref. [1], combined with the physical mass. The errors associated with the fit parameters are statistical followed by systematic, as described in the text. The regulator cutoff for relativistic and HB formalisms are $\Lambda_{(\text{Cov})} = \Lambda_{(\text{Rel})} = 1.0$ GeV and $\Lambda_{(\text{HB})} = 0.8$ GeV, respectively.

| Scheme | C_0 (GeV) | C_2 (GeV ⁻¹) | a_4 (GeV ⁻³) |
|--------------|-------------|----------------------------|----------------------------|
| Covariant | 0.885(1)(7) | 3.59(5)(52) | -0.17(10)(68) |
| Relativistic | 0.882(1)(8) | 3.69(7)(62) | 0.25(13)(112) |
| HB | 0.885(1)(5) | 3.44(5)(42) | -0.29(9)(64) |

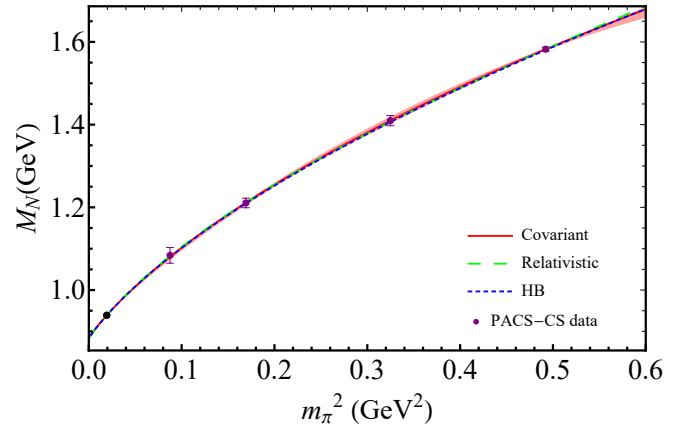


FIG. 3. Fits to the PACS-CS nucleon mass data in the three schemes under consideration, covariant and relativistic formalisms at $\Lambda_{(\text{Cov})} = 1.0$ GeV, and the heavy baryon scheme at $\Lambda_{(\text{HB})} = 0.8$ GeV. The physical nucleon mass (black point) is combined with the lattice results in constraining the fit parameters. The data points are finite-volume corrected but there has been no correction applied for the finite lattice spacing as described in the text. The uncertainties on individual data points are statistical, while the narrow extrapolation band incorporates both statistical and systematic uncertainties.

of C_2 is consistent with the input used in the coefficient of the tadpole contribution of Eq. (18). This is due to the fact that, in the nucleon mass expansion, the renormalized RSC of the m_π^2 is related to one of the tadpole coefficients, specifically $C_2 = -4c_1$. In obtaining the combination of Eq. (18), Refs. [9, 91] quote $c_1 = -0.9^{+0.5}_{-0.2}$ GeV⁻¹. Taking the average value of C_2 in Table II, we find $c_1 = -0.89(1)$ GeV⁻¹ (negligible difference when added in quadrature), which is completely consistent with the input.

In summary, contrary to claims in the literature, the use of HB theory with FRR does allow one to determine model independent LECs using lattice data over a wide range of m_π^2 .

The PACS-CS data set further provides the masses for the other octet baryon (hyperon) masses. Since we restricted the study of the nucleon to dimension-two LECs in SU(2), for the hyperons, we use a form analogous to Eq. (26),

$$\begin{aligned}
 M_\Lambda &= C_0^\Lambda + C_2^\Lambda m_\pi^2 + a_4^\Lambda m_\pi^4 + \tilde{\Sigma}_{\Lambda\Sigma\pi} + \tilde{\Sigma}_{\Lambda NK} + \tilde{\Sigma}_{\Lambda\Xi K} \\
 &\quad + \tilde{\Sigma}_{\Lambda\Lambda\eta} + \tilde{\Sigma}_{\Lambda\Sigma^*\pi} + \tilde{\Sigma}_{\Lambda\Xi^*K}, \\
 M_\Sigma &= C_0^\Sigma + C_2^\Sigma m_\pi^2 + a_4^\Sigma m_\pi^4 + \tilde{\Sigma}_{\Sigma\Sigma\pi} + \tilde{\Sigma}_{\Sigma\Lambda\pi} + \tilde{\Sigma}_{\Sigma NK} \\
 &\quad + \tilde{\Sigma}_{\Sigma\Xi K} + \tilde{\Sigma}_{\Sigma\Sigma\eta} + \tilde{\Sigma}_{\Sigma\Sigma^*\pi} + \tilde{\Sigma}_{\Sigma\Delta K} + \tilde{\Sigma}_{\Sigma\Xi^*K} + \tilde{\Sigma}_{\Sigma\Sigma^*\eta}, \\
 M_\Xi &= C_0^\Xi + C_2^\Xi m_\pi^2 + a_4^\Xi m_\pi^4 + \tilde{\Sigma}_{\Xi\Xi\pi} + \tilde{\Sigma}_{\Xi\Lambda K} + \tilde{\Sigma}_{\Xi\Sigma K} \\
 &\quad + \tilde{\Sigma}_{\Xi\Xi\eta} + \tilde{\Sigma}_{\Xi\Xi^*\pi} + \tilde{\Sigma}_{\Xi\Sigma^*K} + \tilde{\Sigma}_{\Xi\Omega K} + \tilde{\Sigma}_{\Xi\Xi^*\eta}, \quad (27)
 \end{aligned}$$

again omitting the $\mathcal{O}(a^2)$ lattice artifact correction. We reiterate that C_i^B and a_i^B are coefficients of the light flavor chiral expansion of the baryon mass and are unique

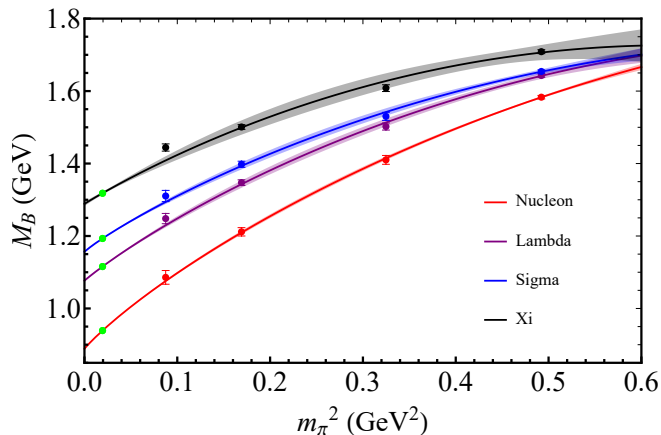


FIG. 4. Fits to the PACS-CS octet baryon mass results in the covariant formalism at $\Lambda_{(\text{Cov})} = 1.0$ GeV, with the inclusion of the physical points (green dots). The data points are finite-volume corrected. The extrapolation bands and errors on individual data points are purely statistical.

to each member of the octet.

In Fig. 4 we see that the baryon mass expansion for the other octet baryons describes the data fairly well. While we only show the covariant fit, the other fits are indistinguishable, similar to those shown in Fig. 3. While not significant for the nucleon, the fact that the strange quark mass used in the PACS-CS simulations is a little large [93] is manifest in Fig. 4. There the extrapolation curves dip down to pass through the experimental values in a manner that leaves the lattice QCD results at the smallest pion mass positioned above the curves.

In Table III we see a similar trend to that found for the nucleon. With a cutoff mass chosen to give a good fit over the large range of m_π^2 provided by PACS-CS, there is very little difference in the renormalized RSCs C_0 and C_2 . Since a_4 is not renormalized, a_4 in itself does

TABLE III. Fits to the RSCs (where $B = \Lambda, \Sigma,$ and Ξ) obtained from the PACS-CS octet baryon mass lattice QCD results of [1], combined with the physical masses. The errors associated with the fit parameters are statistical. The regulator cutoff masses for the relativistic and HB formalisms are $\Lambda_{(\text{Cov})} = \Lambda_{(\text{Rel})} = 1.0$ GeV and $\Lambda_{(\text{HB})} = 0.8$ GeV, respectively.

| Baryon | Scheme | C_0^B (GeV) | C_2^B (GeV $^{-1}$) | a_4^B (GeV $^{-3}$) |
|--------|--------------|---------------|------------------------|------------------------|
| Lambda | Covariant | 1.077(3) | 2.21(11) | -0.78(22) |
| | Relativistic | 1.076(3) | 2.24(11) | -0.71(21) |
| | HB | 1.076(3) | 2.26(10) | -0.76(21) |
| Sigma | Covariant | 1.157(3) | 2.11(10) | -0.70(21) |
| | Relativistic | 1.157(3) | 2.11(10) | -0.65(20) |
| | HB | 1.157(3) | 2.08(10) | -0.74(21) |
| Xi | Covariant | 1.289(6) | 1.64(22) | -0.97(45) |
| | Relativistic | 1.288(6) | 1.65(22) | -0.95(45) |
| | HB | 1.289(6) | 1.62(20) | -0.94(42) |

not represent a physical quantity. However, it is worth noting that variation in a_4 between different schemes in Table III is less than the variation found in Table II. This is largely attributed to the presence of the tadpole term in Eq. (26) which was not included in the fitting form of Eq. (25).

Looking at the differences between the light flavor chiral limit masses, C_0^B and C_0 (recall that we have dropped the superscript N for the nucleon), a simple relationship akin to the constituent quark model emerges. C_0 subtracted from the average of C_0^Λ and C_0^Σ is approximately 200 MeV, and C_0 subtracted from C_0^Ξ is approximately 400 MeV. One can reasonably interpret the differences in these masses arising from the different number of strange quarks.

IV. ANALYSIS OF THE LATEST CLS LATTICE QCD RESULTS FOR THE NUCLEON

Here, we focus on the most recent nucleon mass lattice QCD results from the CLS collaboration [2]. This data set is chosen because it presents a range of accurate lattice QCD results up to $m_\pi^2 = 0.14$ GeV 2 , with the physical mass scale set using the modern gradient flow method [94].

By employing the fit strategy described in Sec. III B on the CLS data set, we find $D_a \approx -6$ GeV fm $^{-2}$ in all the schemes. The results for the fits are shown in Fig. 5 and the renormalized RSCs are provided in Table IV. In performing the fits, we have omitted all data with $L < 2.5$ fm in order to avoid large FVCs.

In the same way from the previous section, we perform a consistency check on C_2 . We find, from Table IV, $c_1 = -0.98(6)$ GeV $^{-1}$ which again is consistent with the input.

The χ_{dof}^2 in all schemes are comparable at approximately 0.62. Again, all the fits are within one standard deviation of one another, and the differences are small.

In relation to the previous section, we also performed an analysis for the combined set of PACS-CS and CLS nucleon lattice data. For this particular case, we allow the coefficient of the tadpole, χC , to also be a fit parameter, constrained by Eq. (18). This is reasonable, as the wide range of m_π^2 covered by the PACS-CS data acts to

TABLE IV. Fits to the nucleon RSCs obtained from the corrected CLS nucleon mass lattice QCD results [2], combined with the physical mass. The errors associated with the fit parameters are statistical followed by systematic, as described in the text. The regulator cutoffs for the covariant, relativistic, and HB formalisms are $\Lambda_{(\text{Cov})} = \Lambda_{(\text{Rel})} = 1.0$ GeV and $\Lambda_{(\text{HB})} = 0.8$ GeV, respectively.

| Scheme | C_0 (GeV) | C_2 (GeV $^{-1}$) | a_4 (GeV $^{-3}$) |
|--------------|-------------|----------------------|----------------------|
| Covariant | 0.879(4)(2) | 3.92(24)(24) | -3.2(20)(22) |
| Relativistic | 0.878(4)(2) | 3.97(24)(27) | -2.7(20)(29) |
| HB | 0.879(4)(2) | 3.85(24)(20) | -4.0(20)(17) |

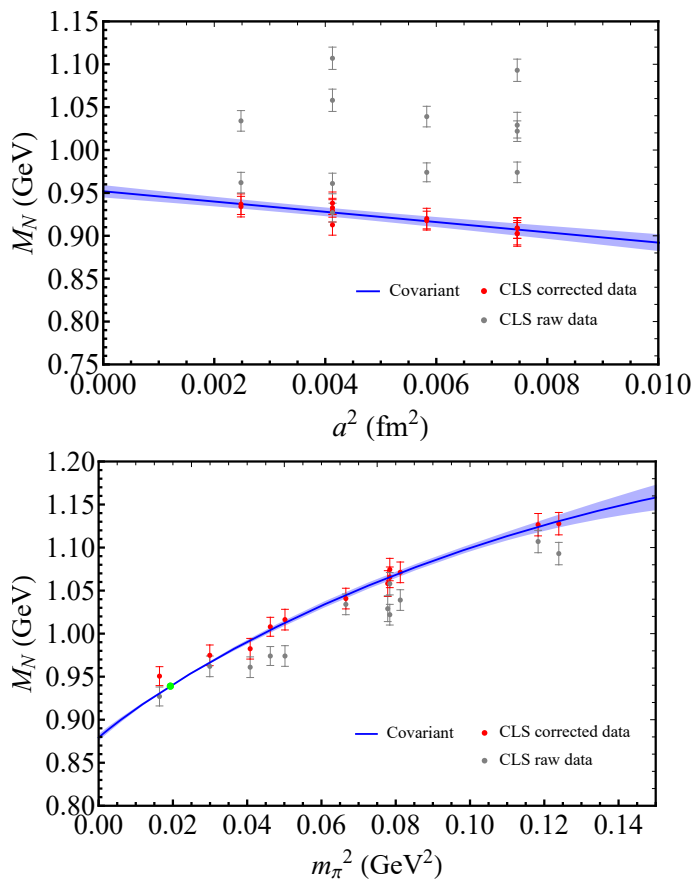


FIG. 5. Fits to the CLS data set in the covariant formalism at $\Lambda_{(\text{Cov})} = 1.0$ GeV. The corrected data refers to the data where finite-volume and $\mathcal{O}(a^2)$ corrections are made. The top panel shows the uncorrected data at various pion masses along with a fit to the corrected data evaluated at $m_\pi^2 = m_\pi^2|_{\text{phys}}$, where $D_a \approx -6$ GeV fm $^{-2}$. The bottom panel shows our fit to the corrected CLS results with the inclusion of the physical point (green dot). The uncertainties on individual data points are statistical while the extrapolation band incorporates both statistical and systematic uncertainties associated with the tadpole contribution.

restrict χC in a meaningful manner. We use the CLS data to correct for the PACS-CS leading lattice artifact (noting that D_a was set to zero for the PACS-CS data in the previous section). Since the variation in the lattice spacing for the PACS-CS data is small, the $\mathcal{O}(a^2)$ correction simply shifts the data points by a constant amount. We find, for the renormalized RSCs and the coefficient of the tadpole, $C_0 = 0.884(4)$ GeV and $C_2 = 3.68(28)$ GeV $^{-1}$, and $\chi C = -1.8(10)$ GeV $^{-1}$, respectively. The χ_{dof}^2 in this case is approximately 0.56. These values are consistent with the those found in the fits presented earlier.

V. COMPARISON OF THE LECS AND THE σ -TERM

A. Comparison of the LECS

Here, we wish to make a comparison between the χ EFT renormalized RSCs of the nucleon extracted using our three FRR schemes and those LECS obtained in earlier χ PT work. In χ PT, the chiral expansion of the nucleon mass in SU(2) is written as [78, 95–97]

$$M_N = m + k_1 m_\pi^2 + k_2 m_\pi^3 + k_3 m_\pi^4 \ln \frac{m_\pi}{\mu} + \dots, \quad (28)$$

where m is the renormalized nucleon mass in the chiral limit, μ is the renormalization parameter, and the coefficients k_i are linear combinations of the renormalized LECS. Explicitly, the k_i are

$$k_1 = -4c_1, \quad k_2 = -\frac{3g_A^2}{32\pi f_\phi^2}, \quad (29)$$

and k_3 is provided in Eq. (17). g_A and f_ϕ are the chiral limit values of the axial-vector coupling constant and pion decay constant, respectively.

We note that the values of k_3 found in the relativistic schemes are different from that found in the HB scheme. Clearly, in the limit $M_N \rightarrow \infty$, the term proportional to g_A^2/M_N vanishes, and

$$\lim_{M_N \rightarrow \infty} \mathcal{A} = \frac{24}{25} g_A^2 \frac{1}{\Delta_{\Delta N}}. \quad (30)$$

The total discrepancy in the coefficient of the NLNA term from the $NN\pi$ and the $N\Delta\pi$ self-energies amounts to 10% between the relativistic and HB formalisms. This difference, in comparison with the uncertainty associated with the tadpole coefficient, χC , is very small.

A comparison is shown in Table V, where we present our (covariant) FRR result from the CLS data set Table IV with earlier χ PT works from Refs. [6] and [7]. These two works include the physical point constraint, but use a different regularization scheme, namely, infrared regularization (IR) and cutoff regularization (CR). The values for k_3 vary greatly with χC . With χC in the range of Eq. (18), $k_3 = -7.4$ to 11.9 GeV $^{-3}$, while the values of Procura *et al.* [6] and Bernard *et al.* [7] yield

TABLE V. Comparison of the renormalized RSCs obtained using FRR in the covariant scheme to analyze the CLS data with those χ PT LECS reported in Refs. [6] and [7]. Note in χ PT notation $C_0 = m$ and $C_2 = k_1$.

| Scheme | C_0 (GeV) | C_2 (GeV $^{-1}$) |
|------------------------|-------------|----------------------|
| FRR result (This work) | 0.879(4)(2) | 3.92(24)(24) |
| Procura IR [6] | 0.883(3) | 3.72(16) |
| Bernard CR [7] | 0.88 | 3.6 (fixed) |

$k_3 = 1.36 \pm 3.29 \text{ GeV}^{-3}$ and $k_3 = 3.82 \text{ GeV}^{-3}$, respectively.

By way of comparison, we also show the results obtained from the CLS collaboration, by fitting a χ PT-inspired form [2]

$$M_N(m_\pi, a, L) = \overset{\circ}{M}_N + Bm_\pi^2 + Cm_\pi^3 + Da^2 + E \frac{m_\pi^3}{m_\pi L} e^{-m_\pi L}. \quad (31)$$

$\overset{\circ}{M}_N$ is the nucleon mass in the chiral limit and the letters B - E represent fit parameters including the LNA term. The lattice artifact correction and FVC are accounted for by the terms proportional to D and E , respectively. Note that in our χ EFT the LNA term is model- and scheme-independent and the coefficient is *not* a fit parameter. Nevertheless, with the above form, we obtain (including the physical point) $\overset{\circ}{M}_N = 0.880(6) \text{ GeV}$, $B = 3.75(46) \text{ GeV}^{-1}$, $C = -4.8(13) \text{ GeV}^{-2}$, $D = -6.0(14) \text{ GeV fm}^{-2}$, and $E = 82(99) \text{ GeV}^{-2}$. We remark that C in this fit is roughly 14% smaller than the correct, model independent value, resulting in a shallow slope of the extrapolation curve near the physical point. Without the physical point constraint in the fit, one would find C to be approximately 2 to 3 times smaller than the χ EFT value. Any extrapolation relying on such a value is unphysical and extracting any physically meaningful observable is difficult. Alternatively, one may fix C to k_2 of χ EFT (see Eq. (29)), and in that case we find $\overset{\circ}{M}_N = 0.875(1) \text{ GeV}$ and $B = 4.07(5) \text{ GeV}^{-1}$ producing reasonable agreement with the values quoted in Table IV.

B. The σ -term

The pion-nucleon sigma term $\sigma_{\pi N}$ is defined as

$$\sigma_{\pi N} = \hat{m} \langle N | \bar{u}u + \bar{d}d | N \rangle, \quad (32)$$

where $\hat{m} = (m_u + m_d)/2$. From the quark mass dependence of the baryon and using the Feynman-Hellmann theorem, one can compute $\sigma_{\pi N}$ by

$$\sigma_{\pi N} = m_\pi^2 \frac{\partial M_N}{\partial m_\pi^2}, \quad (33)$$

at the physical pion mass, where, in our calculation, we use the charged pion mass. The results for the application of Eq. (33) to each of the schemes summarized in Table IV are presented in Table VI. The first set of uncertainties are statistical, while the second set are systematic.

We also show in Fig. 6 a plot of the m_π^2 dependence of $\sigma_{\pi N}$. Again, we show only the result in the covariant scheme, but the curves essentially overlap for the other two schemes, as in Fig. 3. Here, the gradient of the curve starts to flatten at around $m_\pi^2 = 0.1 \text{ GeV}^2$, where the data points become sparse. With points available at larger m_π^2 , as in the PACS-CS data set, we tend to see the curve flattening further out.

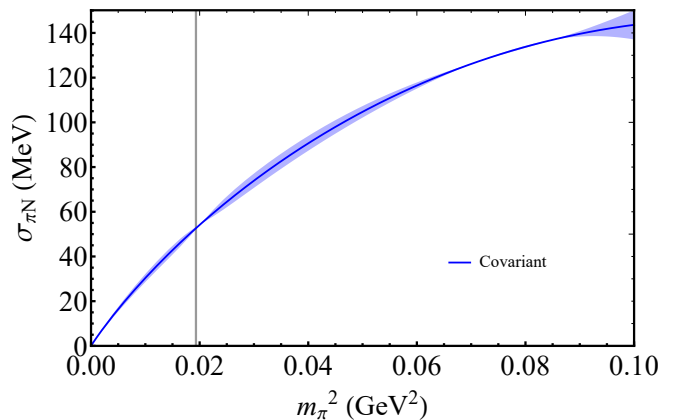


FIG. 6. $\sigma_{\pi N}$ as a function of m_π^2 from the CLS data set fits of Table IV in the covariant formalism at $\Lambda_{(\text{Cov})} = 1.0 \text{ GeV}$. The vertical line represents the physical value of charged m_π^2 . The extrapolation band incorporates both statistical and systematic uncertainties.

In view of the interest in the sigma commutator it is worthwhile to explore the sources of systematic error in some detail.

In Ref. [98], it was suggested that using the neutral pion mass, rather than that of the charged pion, could decrease the value of $\sigma_{\pi N}$ by up to 3 MeV. In our analysis, the changes in $\sigma_{\pi N}$ across all schemes used in Table IV are consistent, with a maximum reduction of 2 MeV.

The explicit tadpole makes a relatively small contribution to $\sigma_{\pi N}$ of order a few MeV. However, the systematic error associated with it is potentially significant because of the large uncertainty in the corresponding coefficient. This error is determined by refitting to the CLS data using fixed values of χC at the upper and lower bound given in Eq. (18) and recalculating $\sigma_{\pi N}$ from the respective fits. In this process we observed a strong correlation between the coefficients k_1 and k_3 which acts to reduce the effect of the systematic uncertainty. Ultimately, the fitted renormalized RSCs are constrained by lattice QCD data, such that a variation in one parameter is mitigated by the other parameters. The net result is a systematic error in $\sigma_{\pi N}$ of approximately $\pm 0.7 \text{ MeV}$ in all schemes.

Further systematic uncertainties in $\sigma_{\pi N}$ may derive

TABLE VI. Pion-nucleon sigma term at the physical point computed from the CLS data set using the fits for each scheme as summarized in Table IV. The first set of uncertainties are statistical and the second set are systematic.

| Scheme | $\sigma_{\pi N}$ (MeV) |
|--------------|------------------------|
| Covariant | $51.7 \pm 3.1 \pm 1.4$ |
| Relativistic | $52.2 \pm 3.2 \pm 1.4$ |
| HB | $51.7 \pm 3.2 \pm 1.4$ |

from the choice of regulator and the corresponding cut-off parameter. References [4] and [5] demonstrated that when lattice data was fit using different regulator functions the renormalized RSCs showed little variation. To test that here, we repeated the fits to the CLS data with three choices of form factor, a monopole, a dipole, and a sharp cutoff. The first two showed no model dependence while the more extreme sharp cutoff gave rise to a 2% variation in the renormalized RSCs. However, even in the latter case the change in $\sigma_{\pi N}$ was just 0.2 MeV. Because the fit is constrained by accurate lattice data, the 2% change in our C_2 was compensated by a change in a_4 .

One may also explore the light quark mass (or m_π^2) dependence of the regulator mass parameter, Λ . We note that the pion cloud has no direct effect on the axial form factor of the nucleon, which is closely related to the pion-nucleon form factor. Thus the variation with pion mass is expected to be slow. Within the MIT bag model the bag radius, which is inversely proportional to the mass parameter Λ in the axial form factor, decreases by just 2% when m_π^2 varies between 0.02 and 0.50 GeV². As a conservative estimate of the effect of the value of Λ varying with pion mass, we have reanalyzed the CLS data allowing for a 5% increase over this mass range. This variation gives rise to a difference of just 0.3 MeV in the value of $\sigma_{\pi N}$.

The remaining input in the fits explored in this work are the coefficients of the pion coupling to the octet and decuplet baryons. A change of $\pm 10\%$ in the coefficient C resulted in a variation of 0.1 MeV in $\sigma_{\pi N}$. A 5% change in f_ϕ gave a variation of 0.3 MeV, and finally the more drastic variation of F and D by $\pm 10\%$ yielded a change in $\sigma_{\pi N}$ of just 0.3 MeV.

To obtain the final systematic error based on all the sources detailed above, we evaluate the sigma commutator at the average of the values obtained with the charged and neutral pion mass, with an uncertainty of ± 1 MeV. The systematic errors arising from all sources are then combined in quadrature, leading to the values shown in Table VI. In Table VII we compare the value of $\sigma_{\pi N}$ calculated here with the values extracted by other methods. Deducing the value from pion-nucleon scattering data [100] may involve a number of complications [103]. As indicated, the preferred value seems to be around 58 MeV with an uncertainty of order 5 MeV [99]. This differs by a surprising amount from direct lattice calculations but is within the uncertainties of most applications of the Feynman-Hellmann theorem. The value found in our analysis, namely $51.7 \pm 3.2 \pm 1.4$ MeV, is compatible with the value extracted from pion-nucleon scattering.

VI. CONCLUSION

We have presented a detailed study of the mass of the nucleon as a function of pion mass using finite range regularization to evaluate the self-energy integrals. The

TABLE VII. Comparison with other determinations of the pion-nucleon sigma commutator.

| Method | $\sigma_{\pi N}$ (MeV) | Ref. |
|-------------------------------------|------------------------|-------|
| Data (πN scattering) | 59.1(3.5) | [98] |
| | 58(5) | [99] |
| | 59(7) | [100] |
| Direct lattice calculation | 45.9(7.4)(2.8) | [101] |
| | 41.6(3.8) | [102] |
| Feynman-Hellmann + lattice data | 45(6) | [16] |
| | 52(3)(8) | [17] |
| | 55(1)(4) | [18] |
| | 44(3)(3) | [22] |
| This work from CLS lattice data [2] | $51.7 \pm 3.2 \pm 1.4$ | |

heavy baryon approximation is compared with a covariant scheme and a relativistic scheme. All three methods produce essentially identical fits to the lattice QCD results from the PACS-CS collaboration [1] over a wide range of pion mass, well beyond the power counting regime. The renormalized residual series coefficients extracted from those fits are independent of the schemes used and agree well with low-energy constants found in earlier studies using χ PT. A similar degree of scheme independence is found when the schemes are applied to the other members of the nucleon octet. This is contrary to the claims of literature where the heavy baryon approximation is deemed unsuitable.

These schemes were then applied to an analysis of the most recent data on the nucleon mass from the CLS Collaboration [2]. Of particular interest is the result that the values of pion-nucleon sigma commutator, $\sigma_{\pi N}$, extracted using all three methods including the uncertainty in the coefficient of the (NLNA) $m_\pi^4 \ln m_\pi$ term in the chiral expansion, are completely consistent. The result is $\sigma_{\pi N} = 51.7 \pm 3.2 \pm 1.4$ MeV. As illustrated in Table VII, this is in reasonable agreement with the value deduced from pion-nucleon scattering data, as well as most applications of the Feynman-Hellmann theorem to lattice data.

ACKNOWLEDGMENTS

This research was undertaken with the assistance of resources from the National Computational Infrastructure (NCI), provided through the National Computational Merit Allocation Scheme. This work was supported by the University of Adelaide and by the Australian Research Council through Discovery Projects DP190102215 and DP210103706 (DBL) and DP230101791 (AWT), as well as through the Australian Research Council Centre of Excellence for Dark Matter Particle Physics (CE200100008).

Appendix A: Effective $SU(3)_L \times SU(3)_R$ chiral Lagrangian

Beginning in the mesonic sector, U is the 3×3 unimodular unitary matrix which contains the meson fields ϕ . In particular,

$$U = \exp\left(i \frac{\phi}{f_\phi}\right) = u^2, \quad (\text{A1})$$

where

$$\phi = \sqrt{2} \begin{bmatrix} \frac{1}{\sqrt{2}}\pi^0 + \frac{1}{\sqrt{6}}\eta & \pi^+ & K^+ \\ \pi^- & -\frac{1}{\sqrt{2}}\pi^0 + \frac{1}{\sqrt{6}}\eta & K^0 \\ K^- & \bar{K}^0 & -\frac{2}{\sqrt{6}}\eta \end{bmatrix}, \quad (\text{A2})$$

with u the unitary square root of U . The investigations of the paper assumes the absence of an external field, so that the covariant derivative $D_\mu U \rightarrow \partial_\mu U$. The explicit chiral symmetry breaking is accounted for in the matrix $\chi = 2B_0 \mathcal{M}$ where $\mathcal{M} = \text{diag}(m_u, m_d, m_s)$ and the parameter B_0 is related to the singlet quark condensate $3F_0^2 B_0 = -\langle 0 | \bar{q}q | 0 \rangle_0$ with F_0 the pseudoscalar decay constant in the chiral limit.

In the octet baryon sector, each baryon field is a four-component Dirac field, and the matrix B follows a similar structure to the meson matrix

$$B = \begin{bmatrix} \frac{1}{\sqrt{2}}\Sigma^0 + \frac{1}{\sqrt{6}}\Lambda & \Sigma^+ & p \\ \Sigma^- & -\frac{1}{\sqrt{2}}\Sigma^0 + \frac{1}{\sqrt{6}}\Lambda & n \\ \Xi^- & \Xi^0 & -\frac{2}{\sqrt{6}}\Lambda \end{bmatrix}. \quad (\text{A3})$$

The covariant derivative of the octet baryon is (again, in the absence of external fields) $D_\mu B = \partial_\mu + [\Gamma_\mu, B]$, where $\Gamma_\mu \equiv \frac{1}{2}(u^\dagger \partial_\mu u + u \partial_\mu u^\dagger)$. With a similar structure to the Γ_μ , the baryon fields couple to the meson fields by the so called chiral vielbein

$$u_\mu \equiv i(u^\dagger \partial_\mu u - u \partial_\mu u^\dagger), \quad (\text{A4})$$

which transforms as an axial-vector under parity transformation. In the NLO Lagrangian, additional chirally invariant structures are possible, and in particular we have $\chi_+ = u^\dagger \chi u^\dagger + u \chi^\dagger u$.

In the decuplet baryon sector, the spin-3/2 decuplet fields are defined by the symmetric flavour tensor T^{ijk} with

$$\begin{aligned} T^{111} &= \Delta^{++}, & T^{112} &= \frac{1}{\sqrt{3}}\Delta^+, \\ T^{122} &= \frac{1}{\sqrt{3}}\Delta^0, & T^{222} &= \Delta^-, \\ T^{113} &= \frac{1}{\sqrt{3}}\Sigma^{*+}, & T^{123} &= \frac{1}{\sqrt{6}}\Sigma^{*0}, & T^{223} &= \frac{1}{\sqrt{3}}\Sigma^{*-}, \\ T^{133} &= \frac{1}{\sqrt{3}}\Xi^{*0}, & T^{233} &= \frac{1}{\sqrt{3}}\Xi^{*-}, & T^{333} &= \Omega^-. \end{aligned} \quad (\text{A5})$$

The covariant derivative is defined by $D_\mu (T_\nu)^{ijk} = \partial_\mu (T_\nu)^{ijk} + (\Gamma_\mu)_l^i (T_\nu)^{ljk} + (\Gamma_\mu)_l^j (T_\nu)^{ilk} + (\Gamma_\mu)_l^k (T_\nu)^{ijl}$.

The propagators of the meson and octet baryon Lagrangian are the usual spin-0 and spin-1/2 Feynman propagators respectively, while the spin-3/2 propagator is a little bit more involved. Here, we simply quote the result [104]

$$\begin{aligned} S_F^{\mu\nu}(p) &= -\frac{\not{p} + M_T}{p^2 - M_T^2 + i\varepsilon} \left[g^{\mu\nu} - \frac{1}{3}\gamma^\mu \gamma^\nu + \frac{(p^\mu \gamma^\nu - \gamma^\mu p^\nu)}{3M_T} \right. \\ &\quad - \frac{2}{3M_T^2} p^\mu p^\nu \left. \right] + \frac{1}{3M_T^2} \frac{1+A}{1+2A} \left[\left(\frac{A}{1+2A} M_T \right. \right. \\ &\quad \left. \left. - \frac{1+A}{2(A+2A)} \not{p} \right) \gamma^\mu \gamma^\nu - \gamma^\mu p^\nu - \frac{A}{1+2A} p^\mu \gamma^\nu \right]. \end{aligned} \quad (\text{A6})$$

In addition, for the leading-order meson-octet-decuplet Lagrangian, the tensor $\Theta^{\mu\nu}$ is defined as

$$\Theta^{\mu\nu} \equiv g^{\mu\nu} + \frac{3A+1}{2}\gamma^\mu \gamma^\nu, \quad (\text{A7})$$

where the choice of the off-shell parameter $A = -1$ simplifies both the propagator and the above tensor, as was done in Eq. (8).

Appendix B: Coupling constants of Lagrangian

Here, we present the coupling constants of the one-loop transitions given in the self-energy expressions Eqs. (7)-(9) determined from the effective Lagrangians Eqs. (2) and (4). These are presented in Tables VIII and IX. For the tadpole couplings, we primarily focus on the $SU(2)$ limit, such that we only have

$$C_{N\pi, \text{tad}} = -3 \left(-2c_1 + \frac{c_2}{4} + c_3 \right) m_\pi^2. \quad (\text{B1})$$

Appendix C: Explicit self-energy contributions

In this section we explicitly show the closed form self-energy contributions in all schemes. We write the internal octet baryon mass as $M_{B'} = M_B + \delta$ where δ is the mass difference between the internal and external octet baryons, and we divide the baryon-baryon-meson self-energy into 2 different parts: terms that produce analytic terms in m_ϕ^2 and terms that produce nonanalytic terms in m_ϕ^2 . Thus, we have, $\Sigma_{BB'\phi} = \Sigma_{BB'\phi}^{(1)} + \Sigma_{BB'\phi}^{(2)}$.

In FRR renormalization, the first part $\Sigma_{BB'\phi}^{(1)}$, containing only the analytic terms, are not generally of interest since they will be subtracted off, see for example, Eq. (15). In fact, if one were to renormalize the chiral expansion of the baryon mass to all orders, everything in $\Sigma_{BB'\phi}^{(1)}$ will be subtracted. Here, we write down all the parts explicitly in all formalisms.

TABLE VIII. Squared coupling constants $C_{BB'\phi}^2$ from two insertions of octet-octet-meson transition.

| N | | Λ | | Σ | | Ξ | |
|-------------|------------------------|---------------|-----------------------|--------------|----------------------|-------------|------------------------|
| $N\pi$ | $\frac{3}{4}(D+F)^2$ | NK | $\frac{1}{6}(D+3F)^2$ | NK | $\frac{1}{2}(D-F)^2$ | ΛK | $\frac{1}{12}(D-3F)^2$ |
| $N\eta$ | $\frac{1}{12}(D-3F)^2$ | $\Lambda\eta$ | $\frac{1}{3}D^2$ | $\Lambda\pi$ | $\frac{1}{3}D^2$ | ΣK | $\frac{3}{4}(D+F)^2$ |
| ΛK | $\frac{1}{12}(D+3F)^2$ | $\Sigma\pi$ | D^2 | $\Sigma\pi$ | $2F^2$ | $\Xi\pi$ | $\frac{3}{4}(D-F)^2$ |
| ΣK | $\frac{3}{4}(D-F)^2$ | ΞK | $\frac{1}{6}(D-3F)^2$ | ΞK | $\frac{1}{2}(D+F)^2$ | $\Xi\eta$ | $\frac{1}{12}(D+3F)^2$ |

TABLE IX. Squared coupling constants $C_{BT'\phi}^2$ from two insertions of octet-decuplet-meson transition.

| N | | Λ | | Σ | | Ξ | |
|-------------|----------------------------|---------------|----------------------------|----------------|----------------------------|-------------|----------------------------|
| $\Delta\pi$ | \mathcal{C}^2 | $\Sigma^*\pi$ | $\frac{3}{4}\mathcal{C}^2$ | ΔK | $\frac{2}{3}\mathcal{C}^2$ | Σ^*K | $\frac{1}{4}\mathcal{C}^2$ |
| Σ^*K | $\frac{1}{4}\mathcal{C}^2$ | Ξ^*K | $\frac{1}{2}\mathcal{C}^2$ | $\Sigma^*\pi$ | $\frac{1}{6}\mathcal{C}^2$ | $\Xi^*\pi$ | $\frac{1}{4}\mathcal{C}^2$ |
| | | | | $\Sigma^*\eta$ | $\frac{1}{4}\mathcal{C}^2$ | $\Xi^*\eta$ | $\frac{1}{4}\mathcal{C}^2$ |
| | | | | Ξ^*K | $\frac{1}{6}\mathcal{C}^2$ | ΩK | $\frac{1}{2}\mathcal{C}^2$ |

$$\begin{aligned}
\Sigma_{BB'\phi}^{(\text{Cov},1)} = & - \frac{C_{BB'\phi}^2 \Lambda^6 (2M_B + \delta)}{96\pi^2 f_\phi^2 M_B (\Lambda^2 - \delta^2) (\Lambda^2 - m_\phi^2)^3 \left((2M_B + \delta)^2 - \Lambda^2 \right)^2} \left\{ \Lambda^2 \left[3\delta^3 (2M_B + \delta)^4 - \delta \Lambda^2 (2M_B + \delta)^2 (7\delta M_B + 9M_B^2 + 6\delta^2) \right. \right. \\
& + \Lambda^4 (11\delta^2 M_B + 13\delta M_B^2 - 2M_B^3 + 3\delta^3) + 2\Lambda^6 M_B \left. \right] \\
& - m_\phi^2 \Lambda^2 \left[\delta (2M_B + \delta)^2 (7\delta M_B + 6M_B^2 + 3\delta^2) + 2\Lambda^2 (-4\delta^2 M_B + \delta M_B^2 + 4M_B^3 - 3\delta^3) + \Lambda^4 (M_B + 3\delta) \right] \\
& + m_\phi^4 M_B \left[\delta (2M_B + \delta)^2 (3M_B + 2\delta) + \Lambda^2 (13\delta M_B + 10M_B^2 + 5\delta^2) - \Lambda^4 \right] \left. \right\} \\
& + \frac{C_{BB'\phi}^2 \Lambda^8 (2M_B + \delta)^2 \arctan \left(\frac{\sqrt{(\delta^2 - \Lambda^2)(\Lambda^2 - (2M_B + \delta)^2)}}{\delta(2M_B + \delta) + \Lambda^2} \right)}{32\pi^2 f_\phi^2 M_B^3 (\Lambda^2 - \delta^2)^{3/2} (\Lambda^2 - m_\phi^2)^4 \left((2M_B + \delta)^2 - \Lambda^2 \right)^{5/2}} \left\{ \delta^6 (2M_B + \delta)^6 - 2\delta^4 \Lambda^2 (2M_B + \delta)^4 (3\delta M_B + 3M_B^2 + 2\delta^2) \right. \\
& + 6\delta^2 \Lambda^4 (2M_B + \delta)^2 (3\delta^3 M_B + 4\delta^2 M_B^2 + 2\delta M_B^3 + M_B^4 + \delta^4) + 2\Lambda^6 (-9\delta^5 M_B - 15\delta^4 M_B^2 - 10\delta^3 M_B^3 + 6\delta M_B^5 + 2M_B^6 - 2\delta^6) \\
& + \Lambda^8 (2\delta^3 M_B - 4\delta M_B^3 - 2M_B^4 + \delta^4) - 2m_\phi^2 \left[\delta^4 (2M_B + \delta)^4 (3\delta M_B + 3M_B^2 + \delta^2) \right. \\
& - 2\delta^2 \Lambda^2 (2M_B + \delta)^2 (3\delta M_B + 3M_B^2 + \delta^2) (3\delta M_B + 3M_B^2 + 2\delta^2) \\
& + 6\Lambda^4 (3\delta M_B + 3M_B^2 + \delta^2) (3\delta^3 M_B + 4\delta^2 M_B^2 + 2\delta M_B^3 + M_B^4 + \delta^4) - 2\Lambda^6 (\delta M_B + M_B^2 + \delta^2) (5\delta M_B + 5M_B^2 + 2\delta^2) \\
& + \Lambda^8 (\delta M_B + M_B^2 + \delta^2) \left. \right] + m_\phi^4 \left[\delta^2 (2M_B + \delta)^2 (6\delta^3 M_B + 12\delta^2 M_B^2 + 12\delta M_B^3 + 6M_B^4 + \delta^4) \right. \\
& - 2\Lambda^2 (3\delta M_B + 3M_B^2 + 2\delta^2) (6\delta^3 M_B + 12\delta^2 M_B^2 + 12\delta M_B^3 + 6M_B^4 + \delta^4) + 6\Lambda^4 (5\delta^3 M_B + 10\delta^2 M_B^2 + 10\delta M_B^3 + 5M_B^4 + \delta^4) \\
& \left. - 2\Lambda^6 (5\delta M_B + 5M_B^2 + 2\delta^2) + \Lambda^8 \right] + 4m_\phi^6 M_B^3 (M_B + \delta)^3 \left. \right\}, \tag{C1}
\end{aligned}$$

$$\begin{aligned} \Sigma_{BB'\phi}^{(\text{Cov},2)} = & \frac{C_{BB'\phi}^2 \Lambda^8 (2M_B + \delta)}{64\pi^2 f_\phi^2 M_B (\Lambda^2 - m_\phi^2)^4} \left\{ 4\delta m_\phi^2 \ln\left(\frac{m_\phi}{\Lambda}\right) + \frac{2(m_\phi^2 - \delta^2)(\delta + 2M_B)}{M_B^2} \left[(\delta(2M_B + \delta) - m_\phi^2) \ln\left(\frac{m_\phi}{\Lambda}\right) \right. \right. \\ & \left. \left. - \sqrt{(m_\phi^2 - \delta^2)((2M_B + \delta)^2 - m_\phi^2)} \arctan\left(\frac{\sqrt{(m_\phi^2 - \delta^2)((2M_B + \delta)^2 - m_\phi^2)}}{\delta(2M_B + \delta) + m_\phi^2}\right) \right] \right\}. \end{aligned} \quad (\text{C2})$$

In a similar fashion, we write $M_{T'} = M_B + \Delta$ for the internal decuplet mass with Δ the mass difference between the external octet and internal decuplet baryon. Again, we divide the self-energies in two different terms.

$$\begin{aligned} \Sigma_{BT'\phi}^{(\text{Cov},1)} = & \frac{C_{BT'\phi}^2 \Lambda^6}{384\pi f_\phi^2 M_B (M_B + \Delta)^2 (\Lambda^2 - \Delta^2) (\Lambda^2 - m_\phi^2)^3} \left\{ \right. \\ & \Lambda^2 \left[2\Lambda^6 - 2\Delta^6 + 4\Delta M_B (-3\Delta^4 + \Delta^2 \Lambda^2 + \Lambda^4) + M_B^2 (-24\Delta^4 + 13\Delta^2 \Lambda^2 + 3\Lambda^4) - 4M_B^3 (4\Delta^3 - 3\Delta \Lambda^2) \right] \\ & + \Lambda^2 m_\phi^2 \left[6(\Delta^4 - \Lambda^4) + 4M_B (5\Delta^3 - 3\Delta \Lambda^2) + M_B^2 (25\Delta^2 - 9\Lambda^2) + 8\Delta M_B^3 \right] \\ & \left. - 2m_\phi^4 \left[3\Delta^2 \Lambda^2 - 3\Lambda^4 + 2\Delta \Lambda^2 M_B + 4\Lambda^2 M_B^2 + 2\Delta M_B^3 \right] \right\} \\ & + \frac{C_{BT'\phi}^2 \Lambda^8}{192\pi^2 f_\phi^2 M_B^3 (M_B + \Delta)^2} \left\{ \ln\left(\frac{M_B + \Delta}{\Lambda}\right) + \frac{\arctan\left(\frac{\sqrt{(\Delta^2 - \Lambda^2)(\Lambda^2 - (2M_B + \Delta)^2)}}{\Delta(2M_B + \Delta) + \Lambda^2}\right)}{(\Lambda^2 - \Delta^2)^{3/2} (\Lambda^2 - m_\phi^2)^4 \sqrt{(2M_B + \Delta)^2 - \Lambda^2}} \right. \\ & - \Delta^6 (2M_B + \Delta)^6 + 2\Delta^4 \Lambda^2 (2M_B + \Delta)^4 (3\Delta M_B + 3M_B^2 + \Delta^2) - 4\Lambda^6 M_B^3 (M_B + \Delta)^3 \\ & + \Lambda^8 (2\Delta^3 M_B - 4\Delta M_B^3 - 2M_B^4 + \Delta^4) - 2\Lambda^{10} (\Delta M_B + M_B^2 + \Delta^2) + \Lambda^{12} - 2m_\phi^2 \left(-\Delta^4 (2M_B + \Delta)^4 (3\Delta M_B + 3M_B^2 + 2\Delta^2) \right. \\ & + 2\Delta^2 \Lambda^2 (2M_B + \Delta)^2 (3\Delta M_B + 3M_B^2 + \Delta^2) (3\Delta M_B + 3M_B^2 + 2\Delta^2) \\ & - \Lambda^4 (3\Delta M_B + 3M_B^2 + 2\Delta^2) (6\Delta^3 M_B + 12\Delta^2 M_B^2 + 12\Delta M_B^3 + 6M_B^4 + \Delta^4) + 2\Lambda^6 (2\Delta^3 M_B - 4\Delta M_B^3 - 2M_B^4 + \Delta^4) \\ & - 4\Lambda^8 (\Delta M_B + M_B^2 + \Delta^2) + 2\Lambda^{10}) + 6m_\phi^4 \left(-\Delta^2 (2M_B + \Delta)^2 (3\Delta^3 M_B + 4\Delta^2 M_B^2 + 2\Delta M_B^3 + M_B^4 + \Delta^4) \right. \\ & + 2\Lambda^2 (3\Delta M_B + 3M_B^2 + \Delta^2) (3\Delta^3 M_B + 4\Delta^2 M_B^2 + 2\Delta M_B^3 + M_B^4 + \Delta^4) - \Lambda^4 M_B (M_B + \Delta) (7\Delta M_B + 7M_B^2 + 3\Delta^2) \\ & \left. - 2\Lambda^6 (\Delta M_B + M_B^2 + \Delta^2) + \Lambda^8 \right) - 2m_\phi^6 \left(-9\Delta^5 M_B - 15\Delta^4 M_B^2 - 10\Delta^3 M_B^3 + 6\Delta M_B^5 + 2M_B^6 - 2\Delta^6 \right. \\ & \left. + 6\Lambda^2 (3\Delta^3 M_B + 4\Delta^2 M_B^2 + 2\Delta M_B^3 + M_B^4 + \Delta^4) - 3\Lambda^4 (3\Delta M_B + 3M_B^2 + 2\Delta^2) + 2\Lambda^6 \right) \left. \right\}, \end{aligned} \quad (\text{C3})$$

$$\begin{aligned} \Sigma_{BT'\phi}^{(\text{Cov},2)} = & \frac{C_{BT'\phi}^2 \Lambda^8}{192\pi^2 f_\phi^2 M_B (M_B + \Delta)^2 (\Lambda^2 - m_\phi^2)^4} \left\{ 2m_\phi^2 \ln\left(\frac{m_\phi}{\Lambda}\right) \left[\Delta (2M_B + \Delta)^3 + m_\phi^2 (-6\Delta M_B - 7M_B^2 - 2\Delta^2) + m_\phi^4 \right] \right. \\ & + \frac{1}{M_B^2} (m_\phi^2 - \Delta^2) ((2M_B + \Delta)^2 - m_\phi^2)^2 \left[\ln\left(\frac{m_\phi}{\Lambda}\right) (\Delta (2M_B + \Delta) - m_\phi^2) \right. \\ & \left. \left. - \sqrt{(m_\phi^2 - \Delta^2)((2M_B + \Delta)^2 - m_\phi^2)} \arctan\left(\frac{\sqrt{(m_\phi^2 - \Delta^2)((2M_B + \Delta)^2 - m_\phi^2)}}{\Delta(2M_B + \Delta) + m_\phi^2}\right) \right] \right\}. \end{aligned} \quad (\text{C4})$$

The explicit nucleon-tadpole self-energy contribution in the covariant formalism is

$$\Sigma_{N\pi,\text{tad}}^{(\text{Cov})} = -\frac{\chi C \Lambda^4 m_\pi^2}{32\pi^2 f_\pi^2 (\Lambda^2 - m_\pi^2)^4} \left[2\Lambda^6 + 3\Lambda^4 m_\pi^2 - 6\Lambda^2 m_\pi^4 + m_\pi^6 + 12\Lambda^4 m_\pi^2 \ln\left(\frac{m_\pi}{\Lambda}\right) \right]. \quad (\text{C5})$$

Here, we present the self-energies in the relativistic scheme

$$\begin{aligned}
\Sigma_{BB'\phi}^{(\text{Rel},1)} = & \frac{C_{BB'\phi}^2 \Lambda^4 (\delta + 2M_B)}{192\pi^2 f_\phi^2 (\Lambda^2 - m_\phi^2)^3 ((M_B + \delta)^2 - \Lambda^2)^3 (m_\phi^2 - \delta^2)(m_\phi^2 - (2M_B + \delta)^2) + 4\Lambda^2 M_B^2} \left\{ \right. \\
& + M_B^{11} (M_B + \delta) (m_\phi^2 - \Lambda^2)^3 (-10\Lambda^2 (M_B + \delta)^2 + 3(M_B + \delta)^4 - 8\Lambda^4) \\
& + M_B (M_B + \delta) (m_\phi^2 - \Lambda^2) ((M_B + \delta)^2 - m_\phi^2)^5 \left[14\Lambda^6 m_\phi^2 - 8\Lambda^4 m_\phi^4 - 2(10\Lambda^6 - 9\Lambda^4 m_\phi^2 + 5\Lambda^2 m_\phi^4) (\delta + M_B)^2 \right. \\
& + (5\Lambda^4 - 2\Lambda^2 m_\phi^2 + 3m_\phi^4) (\delta + M_B)^4 \left. \right] + M_B^9 (M_B + \delta) (m_\phi^2 - \Lambda^2) \left[2\Lambda^4 (-56\Lambda^6 + 128\Lambda^4 m_\phi^2 - 95\Lambda^2 m_\phi^4 + 20m_\phi^6) \right. \\
& + 2(-12\Lambda^8 + 61\Lambda^6 m_\phi^2 - 65\Lambda^4 m_\phi^4 + 25\Lambda^2 m_\phi^6) (\delta + M_B)^2 + (68\Lambda^6 - 175\Lambda^4 m_\phi^2 + 104\Lambda^2 m_\phi^4 - 15m_\phi^6) (\delta + M_B)^4 \\
& + (-7\Lambda^4 + 22\Lambda^2 m_\phi^2 - 9m_\phi^4) (\delta + M_B)^6 \left. \right] + 2M_B^7 (M_B + \delta) (m_\phi^2 - \Lambda^2) \left[\right. \\
& - 4\Lambda^4 (88\Lambda^8 - 204\Lambda^6 m_\phi^2 + 170\Lambda^4 m_\phi^4 - 61\Lambda^2 m_\phi^6 + 10m_\phi^8) + 2\Lambda^2 (232\Lambda^8 - 346\Lambda^6 m_\phi^2 + 81\Lambda^4 m_\phi^4 + 82\Lambda^2 m_\phi^6 - 25m_\phi^8) (\delta + M_B)^2 \\
& + 3(-68\Lambda^8 + 40\Lambda^6 m_\phi^2 + 37\Lambda^4 m_\phi^4 - 38\Lambda^2 m_\phi^6 + 5m_\phi^8) (\delta + M_B)^4 + 2(9\Lambda^6 + 35\Lambda^4 m_\phi^2 - 23\Lambda^2 m_\phi^4 + 3m_\phi^6) (\delta + M_B)^6 \\
& - (\Lambda^4 + 14\Lambda^2 m_\phi^2 - 3m_\phi^4) (\delta + M_B)^8 \left. \right] + \Lambda^2 (m_\phi^2 - (M_B + \delta)^2)^6 \left[8\Lambda^8 + m_\phi^4 (\delta + M_B)^4 + 10\Lambda^6 (m_\phi^2 + (\delta + M_B)^2) \right. \\
& + 17\Lambda^2 m_\phi^2 (\delta + M_B)^2 (m_\phi^2 + (\delta + M_B)^2) - 3\Lambda^4 (m_\phi^4 + 19m_\phi^2 (\delta + M_B)^2 + (\delta + M_B)^4) \left. \right] + M_B^{10} \left[-16\Lambda^{12} - 6m_\phi^6 (\delta + M_B)^6 \right. \\
& + 48\Lambda^{10} (m_\phi^2 + (\delta + M_B)^2) + 13\Lambda^2 m_\phi^4 (\delta + M_B)^4 (m_\phi^2 + (\delta + M_B)^2) - 4\Lambda^8 (7m_\phi^4 + 36m_\phi^2 (\delta + M_B)^2 + 7(\delta + M_B)^4) \\
& - 3\Lambda^4 m_\phi^2 (\delta + M_B)^2 (11m_\phi^4 + 8m_\phi^2 (\delta + M_B)^2 + 11(\delta + M_B)^4) \\
& + \Lambda^6 (m_\phi^2 + (\delta + M_B)^2) (11m_\phi^4 + 73m_\phi^2 (\delta + M_B)^2 + 11(\delta + M_B)^4) \left. \right] - M_B^2 ((M_B + \delta)^2 - m_\phi^2)^4 \left[\right. \\
& - 96\Lambda^{12} + 6m_\phi^6 (\delta + M_B)^6 - 72\Lambda^{10} (m_\phi^2 + (\delta + M_B)^2) - 9\Lambda^2 m_\phi^4 (\delta + M_B)^4 (m_\phi^2 + (\delta + M_B)^2) \\
& - \Lambda^6 (m_\phi^2 + (\delta + M_B)^2) (23m_\phi^4 + 557m_\phi^2 (\delta + M_B)^2 + 23(\delta + M_B)^4) + 4\Lambda^8 (29m_\phi^4 + 194m_\phi^2 (\delta + M_B)^2 + 29(\delta + M_B)^4) \\
& + \Lambda^4 m_\phi^2 (\delta + M_B)^2 (101m_\phi^4 + 248m_\phi^2 (\delta + M_B)^2 + 101(\delta + M_B)^4) \left. \right] - M_B^3 (M_B + \delta) (m_\phi^2 - \Lambda^2) ((M_B + \delta)^2 - m_\phi^2)^3 \left[\right. \\
& 15m_\phi^6 (\delta + M_B)^4 + 9m_\phi^4 (\delta + M_B)^6 + 24\Lambda^8 (-7m_\phi^2 + 10(\delta + M_B)^2) \\
& - 2\Lambda^2 m_\phi^2 (\delta + M_B)^2 (25m_\phi^4 + 46m_\phi^2 (\delta + M_B)^2 + (\delta + M_B)^4) - 2\Lambda^6 (-92m_\phi^4 + 121m_\phi^2 (\delta + M_B)^2 + 91(\delta + M_B)^4) \\
& + \Lambda^4 (-40m_\phi^6 + 124m_\phi^4 (\delta + M_B)^2 + 187m_\phi^2 (\delta + M_B)^4 + 17(\delta + M_B)^6) \left. \right] \\
& + 2M_B^5 (M_B + \delta) (m_\phi^2 - \Lambda^2) ((M_B + \delta)^2 - m_\phi^2) \left[-192\Lambda^{12} + 24\Lambda^{10} (27m_\phi^2 + (\delta + M_B)^2) \right. \\
& + 2\Lambda^2 m_\phi^2 (\delta + M_B)^2 (5m_\phi^2 + 3(\delta + M_B)^2) (-5m_\phi^4 - 8m_\phi^2 (\delta + M_B)^2 + (\delta + M_B)^4) \\
& + 3m_\phi^4 (\delta + M_B)^4 (5m_\phi^4 + 2m_\phi^2 (\delta + M_B)^2 + (\delta + M_B)^4) + 4\Lambda^8 (-160m_\phi^4 - 79m_\phi^2 (\delta + M_B)^2 + 53(\delta + M_B)^4) \\
& + 2\Lambda^6 (121m_\phi^6 + 54m_\phi^4 (\delta + M_B)^2 - 63m_\phi^2 (\delta + M_B)^4 - 64(\delta + M_B)^6) \\
& + \Lambda^4 (-40m_\phi^8 + 162m_\phi^6 (\delta + M_B)^2 + 117m_\phi^4 (\delta + M_B)^4 + 88m_\phi^2 (\delta + M_B)^6 + 9(\delta + M_B)^8) \left. \right] \\
& + 2M_B^4 ((M_B + \delta)^2 - m_\phi^2)^2 \left[192\Lambda^{14} + 48\Lambda^{12} (m_\phi^2 + (\delta + M_B)^2) + 12m_\phi^6 (\delta + M_B)^6 (m_\phi^2 + (\delta + M_B)^2) \right. \\
& - \Lambda^2 m_\phi^4 (\delta + M_B)^4 (23m_\phi^4 + 98m_\phi^2 (\delta + M_B)^2 + 23(\delta + M_B)^4) - 12\Lambda^{10} (31m_\phi^4 + 134m_\phi^2 (\delta + M_B)^2 + 31(\delta + M_B)^4) \\
& + 3\Lambda^4 m_\phi^2 (\delta + M_B)^2 (m_\phi^2 + (\delta + M_B)^2) (39m_\phi^4 + 122m_\phi^2 (\delta + M_B)^2 + 39(\delta + M_B)^4) \\
& + 2\Lambda^8 (m_\phi^2 + (\delta + M_B)^2) (119m_\phi^4 + 920m_\phi^2 (\delta + M_B)^2 + 119(\delta + M_B)^4) \\
& \left. - \Lambda^6 (31m_\phi^8 + 935m_\phi^6 (\delta + M_B)^2 + 1716m_\phi^4 (\delta + M_B)^4 + 935m_\phi^2 (\delta + M_B)^6 + 31(\delta + M_B)^8) \right]
\end{aligned}$$

$$\begin{aligned}
& + M_B^8 \left[-320\Lambda^{14} + 1024\Lambda^{12} (m_\phi^2 + (\delta + M_B)^2) + 24m_\phi^6 (\delta + M_B)^6 (m_\phi^2 + (\delta + M_B)^2) \right. \\
& - \Lambda^2 m_\phi^4 (\delta + M_B)^4 (51m_\phi^4 + 202m_\phi^2 (\delta + M_B)^2 + 51 (\delta + M_B)^4) \\
& + 6\Lambda^8 (m_\phi^2 + (\delta + M_B)^2) (55m_\phi^4 + 422m_\phi^2 (\delta + M_B)^2 + 55 (\delta + M_B)^4) - 16\Lambda^{10} (57m_\phi^4 + 205m_\phi^2 (\delta + M_B)^2 + 57 (\delta + M_B)^4) \\
& \left. - \Lambda^6 (47m_\phi^8 + 1055m_\phi^6 (\delta + M_B)^2 + 2052m_\phi^4 (\delta + M_B)^4 + 1055m_\phi^2 (\delta + M_B)^6 + 47 (\delta + M_B)^8) \right] \\
& + 2M_B^6 \left[256\Lambda^{16} - 256\Lambda^{14} (m_\phi^2 + (\delta + M_B)^2) - 6m_\phi^6 (\delta + M_B)^6 (3m_\phi^4 + 2m_\phi^2 (\delta + M_B)^2 + 3 (\delta + M_B)^4) \right. \\
& - 24\Lambda^{12} (11m_\phi^4 + 38m_\phi^2 (\delta + M_B)^2 + 11 (\delta + M_B)^4) \\
& + \Lambda^2 m_\phi^4 (\delta + M_B)^4 (m_\phi^2 + (\delta + M_B)^2) (37m_\phi^4 + 126m_\phi^2 (\delta + M_B)^2 + 37 (\delta + M_B)^4) \\
& + 4\Lambda^{10} (m_\phi^2 + (\delta + M_B)^2) (159m_\phi^4 + 428m_\phi^2 (\delta + M_B)^2 + 159 (\delta + M_B)^4) \\
& + 3\Lambda^6 (m_\phi^2 + (\delta + M_B)^2) (13m_\phi^8 + 365m_\phi^6 (\delta + M_B)^2 + 188m_\phi^4 (\delta + M_B)^4 + 365m_\phi^2 (\delta + M_B)^6 + 13 (\delta + M_B)^8) \\
& - 4\Lambda^8 (84m_\phi^8 + 639m_\phi^6 (\delta + M_B)^2 + 614m_\phi^4 (\delta + M_B)^4 + 639m_\phi^2 (\delta + M_B)^6 + 84 (\delta + M_B)^8) \\
& \left. - \Lambda^4 m_\phi^2 (\delta + M_B)^2 (133m_\phi^8 + 574m_\phi^6 (\delta + M_B)^2 + 634m_\phi^4 (\delta + M_B)^4 + 574m_\phi^2 (\delta + M_B)^6 + 133 (\delta + M_B)^8) \right] \Bigg\} \\
& - \frac{C_{BB'\phi}^2 \Lambda^3 (2M_B + \delta)^2 \arctan\left(\frac{\sqrt{(M_B + \delta)^2 - \Lambda^2}}{\Lambda}\right)}{64\pi^2 f_\phi^2 ((M_B + \delta)^2 - \Lambda^2)^{7/2} \left((m_\phi^2 - \delta^2)(m_\phi^2 - (2M_B + \delta)^2) + 4\Lambda^2 M_B^2 \right)^4} \Bigg\{ \\
& (M_B + \delta)^7 (\delta^2 - m_\phi^2)^4 ((2M_B + \delta)^2 - m_\phi^2)^3 \\
& + 2\Lambda^2 (M_B + \delta)^5 (\delta^2 - m_\phi^2)^3 ((2M_B + \delta)^2 - m_\phi^2)^2 \left[-3M_B^2 (\delta^2 - 3m_\phi^2) - 9\delta M_B (\delta^2 - m_\phi^2) + 12\delta M_B^3 + 6M_B^4 - 2(\delta^2 - m_\phi^2)^2 \right] \\
& - 4\Lambda^4 (M_B + \delta)^3 (\delta^2 - m_\phi^2)^2 ((2M_B + \delta)^2 - m_\phi^2) \left[M_B^2 (13\delta^2 - 11m_\phi^2) + 11\delta M_B (\delta^2 - m_\phi^2) + 4\delta M_B^3 + 2M_B^4 + 2(\delta^2 - m_\phi^2)^2 \right] \\
& \times \left[2M_B^2 (\delta^2 + 2m_\phi^2) - 4\delta M_B (\delta^2 - m_\phi^2) + 12\delta M_B^3 + 6M_B^4 - (\delta^2 - m_\phi^2)^2 \right] \\
& + 32\Lambda^6 M_B^2 (M_B + \delta)^3 (\delta^2 - m_\phi^2) \left[4(\delta^2 - m_\phi^2)^4 + 38\delta M_B (\delta^2 - m_\phi^2)^3 + 2M_B^2 (63\delta^2 - 19m_\phi^2) (\delta^2 - m_\phi^2)^2 \right. \\
& + \delta M_B^3 (\delta^2 - m_\phi^2) (185\delta^2 - 176m_\phi^2) + M_B^4 (141\delta^4 - 203\delta^2 m_\phi^2 + 88m_\phi^4) + M_B^5 (131\delta^3 - 27\delta m_\phi^2) + 3M_B^6 (55\delta^2 - 3m_\phi^2) \\
& \left. + 104\delta M_B^7 + 26M_B^8 \right] + 64\Lambda^8 M_B^4 (M_B + \delta)^3 \left[12(\delta^2 - m_\phi^2)^3 + 31\delta M_B (\delta^2 - m_\phi^2)^2 - M_B^2 (\delta^2 - m_\phi^2) (19\delta^2 + 31m_\phi^2) \right. \\
& \left. + 2M_B^3 (50\delta m_\phi^2 - 49\delta^3) + M_B^4 (50m_\phi^2 - 44\delta^2) + 6\delta M_B^5 + 2M_B^6 \right] \\
& - 256\Lambda^{10} M_B^5 (M_B + \delta)^2 \left[M_B^2 (22m_\phi^2 - 20\delta^2) - 22\delta M_B (\delta^2 - m_\phi^2) + 4\delta M_B^3 + 2M_B^4 - 7(\delta^2 - m_\phi^2)^2 \right] \\
& \left. + 512\Lambda^{12} M_B^5 \left[2m_\phi^2 (\delta M_B + M_B^2 + \delta^2) - 2\delta^3 M_B + 4\delta M_B^3 + 2M_B^4 - \delta^4 - m_\phi^4 \right] \right\}, \tag{C6}
\end{aligned}$$

$$\begin{aligned}
\Sigma_{BB'\phi}^{(\text{Rel},2)} = & \frac{C_{BB'\phi}^2 \Lambda^3 (2M_B + \delta)}{64\pi^2 f_\phi^2 \left((m_\phi^2 - \delta^2)(m_\phi^2 - (2M_B + \delta)^2) + 4\Lambda^2 M_B^2 \right)^4} \left(-512\Lambda^5 M_B^5 \arctan \left(\frac{\sqrt{(m_\phi^2 - \delta^2)((2M_B + \delta)^2 - m_\phi^2)}}{\delta(2M_B + \delta) + m_\phi^2} \right) \right. \\
& \times (2M_B + \delta) (m_\phi^2 - \delta^2)^{3/2} \sqrt{(2M_B + \delta)^2 - m_\phi^2} + \frac{1}{(m_\phi^2 - \Lambda^2)^{7/2}} \arctan \left(\frac{\sqrt{m_\phi^2 - \Lambda^2}}{\Lambda} \right) \left\{ \right. \\
& - m_\phi^8 (m_\phi^2 - \delta^2)^4 ((2M_B + \delta)^2 - m_\phi^2)^3 \\
& + 2\Lambda^2 m_\phi^6 (m_\phi^2 - \delta^2)^3 ((2M_B + \delta)^2 - m_\phi^2)^2 \left[6M_B^2 (2\delta^2 - 3m_\phi^2) + 9\delta M_B (\delta^2 - m_\phi^2) + 4\delta M_B^3 + 2(m_\phi^2 - \delta^2)^2 \right] \\
& + 4\Lambda^4 m_\phi^4 (m_\phi^2 - \delta^2)^2 (m_\phi^2 - (2M_B + \delta)^2) \left[M_B^2 (4\delta^2 - 10m_\phi^2) + 4\delta M_B (\delta^2 - m_\phi^2) + (m_\phi^2 - \delta^2)^2 \right] \\
& \times \left[M_B^2 (20\delta^2 - 18m_\phi^2) + 11\delta M_B (\delta^2 - m_\phi^2) + 12\delta M_B^3 + 2(m_\phi^2 - \delta^2)^2 \right] \\
& - 32\Lambda^6 M_B^2 m_\phi^4 (m_\phi^2 - \delta^2) \left[4(m_\phi^2 - \delta^2)^4 + 38\delta M_B (\delta^2 - m_\phi^2)^3 - 8M_B^2 (m_\phi^2 - \delta^2)^2 (7m_\phi^2 - 18\delta^2) \right. \\
& \left. + \delta M_B^3 (m_\phi^2 - \delta^2) (263m_\phi^2 - 272\delta^2) + 2M_B^4 (128\delta^4 - 190\delta^2 m_\phi^2 + 75m_\phi^4) + M_B^5 (96\delta^3 - 60\delta m_\phi^2) \right] \\
& + 64\Lambda^8 M_B^4 m_\phi^4 \left[M_B^3 (70\delta m_\phi^2 - 68\delta^3) + 31\delta M_B (m_\phi^2 - \delta^2)^2 + 10M_B^2 (m_\phi^2 - \delta^2) (2\delta^2 + 3m_\phi^2) - 12(m_\phi^2 - \delta^2)^3 \right] \\
& - 256\Lambda^{10} M_B^5 m_\phi^2 \left[M_B^2 (30\delta m_\phi^2 - 28\delta^3) + M_B (-28\delta^4 + 34\delta^2 m_\phi^2 - 6m_\phi^4) - 7\delta (m_\phi^2 - \delta^2)^2 \right] \\
& \left. + 512\Lambda^{12} M_B^5 \left[M_B^2 (6\delta m_\phi^2 - 4\delta^3) - 2M_B (2\delta^4 - 3\delta^2 m_\phi^2 + m_\phi^4) - \delta (m_\phi^2 - \delta^2)^2 \right] \right\}, \tag{C7}
\end{aligned}$$

$$\begin{aligned}
\Sigma_{BT'\phi}^{(\text{Rel},1)} = & \frac{C_{BT'\phi}^2 \Lambda^6 M_B^2}{288\pi^2 f_\phi^2 (m_\phi^2 - \Lambda^2)^3 (M_B + \Delta)^2 ((M_B + \Delta)^2 - \Lambda^2)^3 \left((m_\phi^2 - \Delta^2)(m_\phi^2 - (2M_B + \Delta)^2) + 4\Lambda^2 M_B^2 \right)^3} \left\{ \right. \\
& 128\Lambda^{14} M_B^6 (2\Delta + 3M_B) + \Lambda^2 m_\phi^2 (M_B + \Delta)^3 (\Delta^2 - m_\phi^2) ((2M_B + \Delta)^2 - m_\phi^2)^2 \left[\right. \\
& - 16(m_\phi^2 - \Delta^2)^3 (\Delta^2 + m_\phi^2) + 7\Delta M_B (m_\phi^2 - \Delta^2)^2 (16\Delta^2 + m_\phi^2) M_B^2 + (m_\phi^2 - \Delta^2)^2 (304\Delta^2 + 7m_\phi^2) \\
& \left. + (400\Delta^5 - 830\Delta^3 m_\phi^2 + 334\Delta m_\phi^4) M_B^3 + 2(128\Delta^4 - 287\Delta^2 m_\phi^2 + 63m_\phi^4) M_B^4 + 32\Delta (2\Delta^2 - 5m_\phi^2) M_B^5 \right] \\
& + 16\Lambda^{12} M_B^3 \left[-6(m_\phi^2 - \Delta^2)^3 + 60\Delta M_B (m_\phi^2 - \Delta^2)^2 + 69M_B^2 (3\Delta^4 - 4\Delta^2 m_\phi^2 + m_\phi^4) + 6\Delta M_B^3 (59\Delta^2 - 43m_\phi^2) \right. \\
& \left. + M_B^4 (322\Delta^2 - 70m_\phi^2) + 136\Delta M_B^5 + 10M_B^6 \right] - 4\Lambda^{10} M_B^2 \left[-12\Delta (m_\phi^2 - \Delta^2)^4 - 3M_B (m_\phi^2 - \Delta^2)^3 (27m_\phi^2 - 17\Delta^2) \right. \\
& + 6\Delta M_B^2 (m_\phi^2 - \Delta^2)^2 (3\Delta^2 + 73m_\phi^2) + 2M_B^3 (229\Delta^6 - 75\Delta^4 m_\phi^2 - 291\Delta^2 m_\phi^4 + 137m_\phi^6) \\
& + 8M_B^4 (151\Delta^5 - 101\Delta^3 m_\phi^2 + 46\Delta m_\phi^4) + 8M_B^5 (243\Delta^4 + 50\Delta^2 m_\phi^2 + 64m_\phi^4) + 4M_B^6 (559\Delta^3 + 385\Delta m_\phi^2) \\
& \left. + 4M_B^7 (391\Delta^2 + 155m_\phi^2) + 480\Delta M_B^8 + 16M_B^9 \right] - \Lambda^4 (M_B + \Delta) ((2M_B + \Delta)^2 - m_\phi^2) \left[\right. \\
& - (m_\phi^2 - \Delta^2)^5 (4\Delta^4 + 61\Delta^2 m_\phi^2 + 4m_\phi^4) + \Delta M_B (m_\phi^2 - \Delta^2)^4 (52\Delta^4 + 616\Delta^2 m_\phi^2 - 125m_\phi^4) \\
& - 2M_B^2 (m_\phi^2 - \Delta^2)^3 (148\Delta^6 + 1133\Delta^4 m_\phi^2 - 991\Delta^2 m_\phi^4 + 34m_\phi^6) \\
& + 4\Delta M_B^3 (m_\phi^2 - \Delta^2)^2 (242\Delta^6 + 705\Delta^4 m_\phi^2 - 2040\Delta^2 m_\phi^4 + 547m_\phi^6) \\
& + M_B^4 + (m_\phi^2 - \Delta^2) (-2004\Delta^8 + 4283\Delta^6 m_\phi^2 + 9439\Delta^4 m_\phi^4 - 10391\Delta^2 m_\phi^6 + 833m_\phi^8) \\
& + 4\Delta M_B^5 (681\Delta^8 - 4943\Delta^6 m_\phi^2 + 4147\Delta^4 m_\phi^4 + 1651\Delta^2 m_\phi^6 - 1524m_\phi^8) \\
& \left. - 4M_B^6 (-608\Delta^8 + 6829\Delta^6 m_\phi^2 - 7877\Delta^4 m_\phi^4 + 1211\Delta^2 m_\phi^6 + 397m_\phi^8) + 8\Delta M_B^7 (172\Delta^6 - 2557\Delta^4 m_\phi^2 + 3074\Delta^2 m_\phi^4 - 653m_\phi^6) \right\}
\end{aligned}$$

$$\begin{aligned}
& -16M_B^8 (-28\Delta^6 + 504\Delta^4 m_\phi^2 - 573\Delta^2 m_\phi^4 + 85m_\phi^6) + 16M_B^9 (4\Delta^5 - 82\Delta^3 m_\phi^2 + 81\Delta m_\phi^4) \Big] \\
& + 2\Lambda^8 \left[2\Delta (m_\phi^2 - \Delta^2)^6 + 3M_B (m_\phi^2 - 9\Delta^2) (m_\phi^2 - \Delta^2)^5 + 6\Delta M_B^2 (m_\phi^2 - \Delta^2)^4 (41\Delta^2 + 5m_\phi^2) \right. \\
& + 2M_B^3 (m_\phi^2 - \Delta^2)^3 (-801\Delta^4 - 257\Delta^2 m_\phi^2 + 16m_\phi^4) + 12\Delta M_B^4 (m_\phi^2 - \Delta^2)^2 (559\Delta^4 + 2\Delta^2 m_\phi^2 - 115m_\phi^4) \\
& - 3M_B^5 (m_\phi^2 - \Delta^2) (5933\Delta^6 - 4579\Delta^4 m_\phi^2 - 1145\Delta^2 m_\phi^4 + 263m_\phi^6) + 8M_B^6 (3792\Delta^7 - 6858\Delta^5 m_\phi^2 + 2691\Delta^3 m_\phi^4 + 395\Delta m_\phi^6) \\
& + 24M_B^7 (1395\Delta^6 - 2626\Delta^4 m_\phi^2 + 1227\Delta^2 m_\phi^4 + 52m_\phi^6) + 24M_B^8 (1000\Delta^5 - 1719\Delta^3 m_\phi^2 + 867\Delta m_\phi^4) \\
& \left. + 8M_B^9 (1440\Delta^4 - 1447\Delta^2 m_\phi^2 + 707m_\phi^4) + 384\Delta M_B^{10} (11\Delta^2 + m_\phi^2) + 96M_B^{11} (14\Delta^2 + 5m_\phi^2) + 256\Delta M_B^{12} \right] \\
& + \Lambda^6 \left[15\Delta (m_\phi^2 - \Delta^2)^6 (\Delta^2 + m_\phi^2) + M_B (m_\phi^2 - \Delta^2)^5 (-227\Delta^4 - 158\Delta^2 m_\phi^2 + 28m_\phi^4) \right. \\
& + 2\Delta M_B^2 (m_\phi^2 - \Delta^2)^4 (727\Delta^4 - 179\Delta^2 m_\phi^2 - 260m_\phi^4) - 2M_B^3 (m_\phi^2 - \Delta^2)^3 (2485\Delta^6 - 5262\Delta^4 m_\phi^2 - 336\Delta^2 m_\phi^4 + 173m_\phi^6) \\
& + \Delta M_B^4 (m_\phi^2 - \Delta^2)^2 (8747\Delta^6 - 55897\Delta^4 m_\phi^2 + 25673\Delta^2 m_\phi^4 + 1317m_\phi^6) \\
& + M_B^5 (m_\phi^2 - \Delta^2) (-2159\Delta^8 + 142822\Delta^6 m_\phi^2 - 163232\Delta^4 m_\phi^4 + 32010\Delta^2 m_\phi^6 + 687m_\phi^8) \\
& + 8M_B^6 (-3335\Delta^9 - 22665\Delta^7 m_\phi^2 + 52053\Delta^5 m_\phi^4 - 28459\Delta^3 m_\phi^6 + 2550\Delta m_\phi^8) \\
& + 4M_B^7 (-17087\Delta^8 - 28744\Delta^6 m_\phi^2 + 88446\Delta^4 m_\phi^4 - 42408\Delta^2 m_\phi^6 + 1257m_\phi^8) \\
& - 32M_B^8 (2809\Delta^7 - 423\Delta^5 m_\phi^2 - 5124\Delta^3 m_\phi^4 + 2346\Delta m_\phi^6) - 16M_B^9 (4535\Delta^6 - 5148\Delta^4 m_\phi^2 - 1242\Delta^2 m_\phi^4 + 939m_\phi^6) \\
& \left. - 32M_B^{10} (1132\Delta^5 - 1867\Delta^3 m_\phi^2 + 423\Delta m_\phi^4) - 32M_B^{11} (322\Delta^4 - 570\Delta^2 m_\phi^2 + 129m_\phi^4) + 640M_B^{12} (3\Delta m_\phi^2 - 2\Delta^3) \right] \\
& + 3m_\phi^4 (M_B + \Delta)^5 (m_\phi^2 - \Delta^2)^2 ((2M_B + \Delta)^2 - m_\phi^2)^3 (\Delta (M_B + \Delta) - m_\phi^2) \Big\} \\
& - \frac{C_{BT'\phi}^2 \Lambda^3 \arctan\left(\frac{\sqrt{(M_B + \Delta)^2 - \Lambda^2}}{\Lambda}\right)}{96\pi^2 f_\phi^2 (M_B + \Delta)^2 ((M_B + \Delta)^2 - \Lambda^2)^{7/2} \left((m_\phi^2 - \Delta^2)(m_\phi^2 - (2M_B + \Delta)^2) + 4\Lambda^2 M_B^2 \right)^4} \Big\{ \\
& (M_B + \Delta)^7 (m_\phi^2 - \Delta^2)^3 ((2M_B + \Delta)^2 - m_\phi^2)^4 \\
& - 2\Lambda^2 (M_B + \Delta)^5 (m_\phi^2 - \Delta^2)^2 ((2M_B + \Delta)^2 - m_\phi^2)^3 \left[-3(m_\phi^2 - \Delta^2)^2 + 7\Delta M_B (m_\phi^2 - \Delta^2) + M_B^2 (11\Delta^2 + 7m_\phi^2) \right. \\
& \left. + 36\Delta M_B^3 + 18M_B^4 \right] + 24\Lambda^4 M_B^2 (M_B + \Delta)^5 (\Delta^2 - m_\phi^2) ((2M_B + \Delta)^2 - m_\phi^2)^2 \left[3M_B^2 (9\Delta^2 - 7m_\phi^2) + 21\Delta M_B (\Delta^2 - m_\phi^2) \right. \\
& \left. + 4(m_\phi^2 - \Delta^2)^2 + 12\Delta M_B^3 + 6M_B^4 \right] + 16\Lambda^6 M_B^3 (M_B + \Delta)^4 ((2M_B + \Delta)^2 - m_\phi^2) \left[35(m_\phi^2 - \Delta^2)^3 \right. \\
& \left. - 174\Delta M_B (m_\phi^2 - \Delta^2)^2 - 6M_B^2 (50\Delta^4 - 79\Delta^2 m_\phi^2 + 29m_\phi^4) + 4M_B^3 (63\Delta m_\phi^2 - 62\Delta^3) + 6M_B^4 (21m_\phi^2 - 19\Delta^2) \right. \\
& \left. + 12\Delta M_B^5 + 4M_B^6 \right] + 64\Lambda^8 M_B^3 (M_B + \Delta)^2 \left[-7(m_\phi^2 - \Delta^2)^4 + 70\Delta M_B (m_\phi^2 - \Delta^2)^3 + 70M_B^2 (m_\phi^2 - 4\Delta^2) (m_\phi^2 - \Delta^2)^2 \right. \\
& \left. - 4M_B^3 (146\Delta^5 - 251\Delta^3 m_\phi^2 + 105\Delta m_\phi^4) + M_B^4 (-688\Delta^4 + 912\Delta^2 m_\phi^2 - 210m_\phi^4) + M_B^5 (492\Delta m_\phi^2 - 436\Delta^3) \right. \\
& \left. + 4M_B^6 (41m_\phi^2 - 20\Delta^2) + 56\Delta M_B^7 + 14M_B^8 \right] + 128\Lambda^{10} M_B^3 \left[-(m_\phi^2 - \Delta^2)^4 + 10\Delta M_B (m_\phi^2 - \Delta^2)^3 \right. \\
& \left. + 10M_B^2 (m_\phi^2 - 4\Delta^2) (m_\phi^2 - \Delta^2)^2 - 20M_B^3 (4\Delta^5 - 7\Delta^3 m_\phi^2 + 3\Delta m_\phi^4) - 10M_B^4 (8\Delta^4 - 12\Delta^2 m_\phi^2 + 3m_\phi^4) \right. \\
& \left. + 20M_B^5 (3\Delta m_\phi^2 - \Delta^3) + 20M_B^6 (2\Delta^2 + m_\phi^2) + 40\Delta M_B^7 + 10M_B^8 \right] \Big\}, \tag{C8}
\end{aligned}$$

$$\begin{aligned}
\Sigma_{BT'\phi}^{(\text{Rel},2)} = & \frac{C_{BT'\phi}^2 \Lambda^5 M_B^2}{96\pi^2 f_\phi^2 (M_B + \Delta)^2 \left((m_\phi^2 - \Delta^2)(m_\phi^2 - (2M_B + \Delta)^2) + 4\Lambda^2 M_B^2 \right)^4} \left(\right. \\
& - 128\Lambda^3 M_B^3 (m_\phi^2 - \Delta^2)^{3/2} \left((2M_B + \Delta)^2 - m_\phi^2 \right)^{5/2} \arctan \left(\frac{\sqrt{(m_\phi^2 - \Delta^2)((2M_B + \Delta)^2 - m_\phi^2)}}{\Delta (2M_B + \Delta) + m_\phi^2} \right) \\
& - \frac{1}{(m_\phi^2 - \Lambda^2)^{7/2}} \arctan \left(\frac{\sqrt{m_\phi^2 - \Lambda^2}}{\Lambda} \right) \left\{ \Delta m_\phi^6 (m_\phi^2 - \Delta^2)^3 \left((2M_B + \Delta)^2 - m_\phi^2 \right)^4 \right. \\
& + 2\Lambda^2 m_\phi^4 (m_\phi^2 - \Delta^2)^2 \left((2M_B + \Delta)^2 - m_\phi^2 \right)^3 \left[3\Delta (m_\phi^2 - \Delta^2)^2 + M_B (12\Delta^4 - 17\Delta^2 m_\phi^2 + 5m_\phi^4) - 6M_B^2 (5\Delta m_\phi^2 - 2\Delta^3) \right] \\
& - 24\Lambda^4 M_B^2 m_\phi^4 (m_\phi^2 - \Delta^2) \left((2M_B + \Delta)^2 - m_\phi^2 \right)^2 \left[4\Delta (m_\phi^2 - \Delta^2)^2 - M_B (-16\Delta^4 + 11\Delta^2 m_\phi^2 + 5m_\phi^4) - 2M_B^2 (5\Delta m_\phi^2 - 8\Delta^3) \right] \\
& + 16\Lambda^6 M_B^3 m_\phi^4 \left[-35 (m_\phi^2 - \Delta^2)^4 + 314\Delta M_B (m_\phi^2 - \Delta^2)^3 + 2M_B^2 (m_\phi^2 - \Delta^2)^2 (145m_\phi^2 - 556\Delta^2) \right. \\
& - 4M_B^3 (484\Delta^5 - 843\Delta^3 m_\phi^2 + 359\Delta m_\phi^4) - 8M_B^4 (206\Delta^4 - 283\Delta^2 m_\phi^2 + 75m_\phi^4) + 16M_B^5 (35\Delta m_\phi^2 - 34\Delta^3) \left. \right] \\
& - 64\Lambda^8 M_B^3 m_\phi^2 \left[-7 (m_\phi^2 - \Delta^2)^4 + 70\Delta M_B (m_\phi^2 - \Delta^2)^3 + 70M_B^2 (m_\phi^2 - 4\Delta^2) (m_\phi^2 - \Delta^2)^2 \right. \\
& - 4M_B^3 (140\Delta^5 - 239\Delta^3 m_\phi^2 + 99\Delta m_\phi^4) - 2M_B^4 (280\Delta^4 - 372\Delta^2 m_\phi^2 + 85m_\phi^4) + 16M_B^5 (15\Delta m_\phi^2 - 14\Delta^3) \left. \right] \\
& + 128\Lambda^{10} M_B^3 \left[- (m_\phi^2 - \Delta^2)^4 + 10\Delta M_B (m_\phi^2 - \Delta^2)^3 + 10M_B^2 (m_\phi^2 - 4\Delta^2) (m_\phi^2 - \Delta^2)^2 - 20M_B^3 (4\Delta^5 - 7\Delta^3 m_\phi^2 + 3\Delta m_\phi^4) \right. \\
& \left. \left. - 10M_B^4 (8\Delta^4 - 12\Delta^2 m_\phi^2 + 3m_\phi^4) + 16M_B^5 (3\Delta m_\phi^2 - 2\Delta^3) \right] \right\}, \tag{C9}
\end{aligned}$$

$$\Sigma_{N\pi,\text{tad}}^{(\text{Rel})} = \frac{\chi C \Lambda^3 m_\pi^2}{256\pi^2 f_\pi^2 (\Lambda^2 - m_\pi^2)^{7/2}} \left[\Lambda \sqrt{\Lambda^2 - m_\pi^2} (-8\Lambda^4 - 10\Lambda^2 m_\pi^2 + 3m_\pi^4) + 3m_\pi^2 (8\Lambda^4 - 4\Lambda^2 m_\pi^2 + m_\pi^4) \operatorname{artanh} \left(\frac{\sqrt{\Lambda^2 - m_\pi^2}}{\Lambda} \right) \right]. \tag{C10}$$

Finally, in the HB scheme

$$\begin{aligned}
\Sigma_{BB'\phi}^{(\text{HB},1)} = & - \frac{C_{BB'\phi}^2 \Lambda^5}{384\pi^2 f_\phi^2 (\delta^2 + \Lambda^2 - m_\phi^2)^4} \left\{ 3\pi \left(\Lambda^6 + 9\Lambda^4 (\delta^2 - m_\phi^2) - 9\Lambda^2 (m_\phi^2 - \delta^2)^2 + (m_\phi^2 - \delta^2)^3 \right) \right. \\
& + \frac{48\delta\Lambda (\delta^2 - m_\phi^2)^2 (\delta^2 + \Lambda^2 - m_\phi^2)}{m_\phi^2 - \Lambda^2} \\
& \left. + \frac{2\delta\Lambda (\delta^2 + \Lambda^2 - m_\phi^2)^2 (-28\delta^2\Lambda^4 + 8\Lambda^6 - (21\delta^2 + 67\Lambda^2) m_\phi^4 + (64\delta^2\Lambda^2 + 38\Lambda^4) m_\phi^2 + 21m_\phi^6)}{(m_\phi^2 - \Lambda^2)^3} \right\}, \tag{C11}
\end{aligned}$$

$$\begin{aligned}
\Sigma_{BB'\phi}^{(\text{HB},2)} = & \frac{C_{BB'\phi}^2 \Lambda^8}{64\pi^2 f_\phi^2 (\delta^2 + \Lambda^2 - m_\phi^2)^4} \left\{ 8 (m_\phi^2 - \delta^2)^{3/2} \left[2 \arctan \left(\frac{\delta}{\sqrt{m_\phi^2 - \delta^2}} \right) - \pi \right] \right. \\
& - \frac{\delta}{\Lambda^3 (\Lambda^2 - m_\phi^2)^{7/2}} \operatorname{artanh} \left(\frac{\sqrt{\Lambda^2 - m_\phi^2}}{\Lambda} \right) \left[-16\delta^2 \Lambda^{10} + 8\Lambda^8 (7\delta^2 + 3\Lambda^2) m_\phi^2 + (6\delta^6 \Lambda^2 + 24\delta^4 \Lambda^4 - 34\delta^2 \Lambda^6 - 60\Lambda^8) m_\phi^4 \right. \\
& \left. \left. - (\delta^6 + 27\delta^4 \Lambda^2 + 39\delta^2 \Lambda^4 - 35\Lambda^6) m_\phi^6 + 3(\delta^4 + 12\delta^2 \Lambda^2 + 5\Lambda^4) m_\phi^8 - 3(\delta^2 + 5\Lambda^2) m_\phi^{10} + m_\phi^{12} \right] \right\}. \quad (\text{C12})
\end{aligned}$$

Then observing Eqs. (22) and (23), we note that the expression for the octet-decuplet-meson self-energy will be the same besides the factor of 2/3, and replacing $\delta \rightarrow \Delta$ and $C_{BB'\phi} \rightarrow C_{BT'\phi}$. We further remark that $\Sigma_{N\pi,\text{tad}}^{(\text{Rel})} = \Sigma_{N\pi,\text{tad}}^{(\text{HB})}$.

-
- [1] S. Aoki, K.-I. Ishikawa, N. Ishizuka, T. Izubuchi, D. Kadoh, K. Kanaya, Y. Kuramashi, Y. Namekawa, M. Okawa, Y. Taniguchi, A. Ukawa, N. Ukita, and T. Yoshié (PACS-CS Collaboration), 2 + 1 flavor lattice QCD toward the physical point, *Phys. Rev. D* **79**, 034503 (2009).
- [2] K. Ottnad, D. Djukanovic, H. B. Meyer, G. von Hippel, and H. Wittig, Mass and isovector matrix elements of the nucleon at zero-momentum transfer, *PoS LATTICE2022*, 117 (2023), arXiv:2212.09940 [hep-lat].
- [3] D. B. Leinweber, A. W. Thomas, K. Tsushima, and S. V. Wright, Baryon masses from lattice QCD: Beyond the perturbative chiral regime, *Phys. Rev. D* **61**, 074502 (2000), arXiv:hep-lat/9906027.
- [4] R. D. Young, D. B. Leinweber, and A. W. Thomas, Convergence of chiral effective field theory, *Prog. Part. Nucl. Phys.* **50**, 399 (2003), arXiv:hep-lat/0212031.
- [5] D. B. Leinweber, A. W. Thomas, and R. D. Young, Physical nucleon properties from lattice QCD, *Phys. Rev. Lett.* **92**, 242002 (2004), arXiv:hep-lat/0302020.
- [6] M. Procura, T. R. Hemmert, and W. Weise, Nucleon mass, sigma term, and lattice QCD, *Phys. Rev. D* **69**, 034505 (2004).
- [7] V. Bernard, T. R. Hemmert, and U.-G. Meißner, Cut-off schemes in chiral perturbation theory and the quark mass expansion of the nucleon mass, *Nuclear Physics A* **732**, 149 (2004).
- [8] V. Bernard, T. R. Hemmert, and U.-G. Meißner, Chiral extrapolations and the covariant small scale expansion, *Physics Letters B* **622**, 141 (2005).
- [9] U.-G. Meißner, Quark mass dependence of baryon properties: Foundations and applications, *Nuclear Physics B - Proceedings Supplements* **153**, 170 (2006), proceedings of the Workshop on Computational Hadron Physics.
- [10] K. Goeke, J. Ossmann, P. Schweitzer, and A. Silva, Pion mass dependence of the nucleon mass in the chiral quark soliton model, *The European Physical Journal A - Hadrons and Nuclei* **27**, 77 (2006).
- [11] M. Procura, B. U. Musch, T. Wollenweber, T. R. Hemmert, and W. Weise, Nucleon mass: From lattice QCD to the chiral limit, *Phys. Rev. D* **73**, 114510 (2006).
- [12] W. Armour, C. R. Allton, D. B. Leinweber, A. W. Thomas, and R. D. Young, An Analysis of the nucleon spectrum from lattice partially-quenched QCD, *Nucl. Phys. A* **840**, 97 (2010), arXiv:0810.3432 [hep-lat].
- [13] J. M. M. Hall, D. B. Leinweber, and R. D. Young, Power Counting Regime of Chiral Effective Field Theory and Beyond, *Phys. Rev. D* **82**, 034010 (2010), arXiv:1002.4924 [hep-lat].
- [14] X.-L. Ren, L. S. Geng, J. M. Camalich, J. Meng, and H. Toki, Octet baryon masses in next-to-next-to-next-to-leading order covariant baryon chiral perturbation theory, *Journal of High Energy Physics* **2012**, 73 (2012).
- [15] P. C. Bruns, L. Greil, and A. Schäfer, Chiral extrapolation of baryon mass ratios, *Phys. Rev. D* **87**, 054021 (2013), arXiv:1209.0980 [hep-ph].
- [16] P. E. Shanahan, A. W. Thomas, and R. D. Young, Sigma terms from an SU(3) chiral extrapolation, *Phys. Rev. D* **87**, 074503 (2013), arXiv:1205.5365 [nucl-th].
- [17] L. Alvarez-Ruso, T. Ledwig, J. Martin Camalich, and M. J. Vicente-Vacas, Nucleon mass and pion-nucleon sigma term from a chiral analysis of lattice QCD data, *Phys. Rev. D* **88**, 054507 (2013), arXiv:1304.0483 [hep-ph].
- [18] X.-L. Ren, L.-S. Geng, and J. Meng, Scalar strangeness content of the nucleon and baryon sigma terms, *Phys. Rev. D* **91**, 051502 (2015), arXiv:1404.4799 [hep-ph].
- [19] M. F. M. Lutz, Y. Heo, and X.-Y. Guo, On the convergence of the chiral expansion for the baryon ground-state masses, *Nucl. Phys. A* **977**, 146 (2018), arXiv:1801.06417 [hep-lat].
- [20] G. S. Bali, S. Collins, W. Söldner, and S. Weishäupl (RQCD Collaboration), Leading order mesonic and baryonic su(3) low energy constants from $N_f = 3$ lattice QCD, *Phys. Rev. D* **105**, 054516 (2022).
- [21] M. F. M. Lutz, Y. Heo, and X.-Y. Guo, Low-energy constants in the chiral Lagrangian with baryon octet and decuplet fields from Lattice QCD data on CLS ensembles, *Eur. Phys. J. C* **83**, 440 (2023), arXiv:2301.06837 [hep-lat].
- [22] P. M. Copeland, C.-R. Ji, and W. Melnitchouk, Octet and decuplet baryon σ terms and mass decompositions, *Phys. Rev. D* **107**, 094041 (2023), arXiv:2112.03198 [nucl-th].
- [23] D. B. Leinweber, Quark contributions to baryon magnetic moments in full, quenched and partially quenched QCD, *Phys. Rev. D* **69**, 014005 (2004), arXiv:hep-lat/0211017.
- [24] D. B. Leinweber, S. Boinepalli, I. C. Cloet, A. W. Thomas, A. G. Williams, R. D. Young, J. M. Zan-

- otti, and J. B. Zhang, Precise determination of the strangeness magnetic moment of the nucleon, *Phys. Rev. Lett.* **94**, 212001 (2005), arXiv:hep-lat/0406002.
- [25] D. B. Leinweber, S. Boinepalli, A. W. Thomas, P. Wang, A. G. Williams, R. D. Young, J. M. Zanotti, and J. B. Zhang, Strange electric form-factor of the proton, *Phys. Rev. Lett.* **97**, 022001 (2006), arXiv:hep-lat/0601025.
- [26] J. M. M. Hall, D. B. Leinweber, B. J. Owen, and R. D. Young, Finite-volume corrections to charge radii, *Phys. Lett. B* **725**, 101 (2013), arXiv:1210.6124 [hep-lat].
- [27] J. M. M. Hall, D. B. Leinweber, and R. D. Young, Chiral extrapolations for nucleon electric charge radii, *Phys. Rev. D* **88**, 014504 (2013), arXiv:1305.3984 [hep-lat].
- [28] P. E. Shanahan, A. W. Thomas, R. D. Young, J. M. Zanotti, R. Horsley, Y. Nakamura, D. Pleiter, P. E. L. Rakow, G. Schierholz, and H. Stüben (CSSM, QCDSF/UKQCD), Magnetic form factors of the octet baryons from lattice QCD and chiral extrapolation, *Phys. Rev. D* **89**, 074511 (2014), arXiv:1401.5862 [hep-lat].
- [29] J. M. M. Hall, D. B. Leinweber, and R. D. Young, Chiral extrapolations for nucleon magnetic moments, *Phys. Rev. D* **85**, 094502 (2012), arXiv:1201.6114 [hep-lat].
- [30] J. M. M. Hall, D. B. Leinweber, and R. D. Young, Finite-volume and partial quenching effects in the magnetic polarizability of the neutron, *Phys. Rev. D* **89**, 054511 (2014), arXiv:1312.5781 [hep-lat].
- [31] R. Bignell, J. Hall, W. Kamleh, D. Leinweber, and M. Burkardt, Neutron magnetic polarizability with Landau mode operators, *Phys. Rev. D* **98**, 034504 (2018), arXiv:1804.06574 [hep-lat].
- [32] R. Bignell, W. Kamleh, and D. Leinweber, Magnetic polarizability of the nucleon using a Laplacian mode projection, *Phys. Rev. D* **101**, 094502 (2020), arXiv:2002.07915 [hep-lat].
- [33] R. G. Edwards, G. T. Fleming, P. Hagler, J. W. Negele, K. Orginos, A. V. Pochinsky, D. B. Renner, D. G. Richards, and W. Schroers (LHPC), The Nucleon axial charge in full lattice QCD, *Phys. Rev. Lett.* **96**, 052001 (2006), arXiv:hep-lat/0510062.
- [34] R. Horsley, Y. Nakamura, A. Nobile, P. E. L. Rakow, G. Schierholz, and J. M. Zanotti, Nucleon axial charge and pion decay constant from two-flavor lattice QCD, *Phys. Lett. B* **732**, 41 (2014), arXiv:1302.2233 [hep-lat].
- [35] J. Liang, Y.-B. Yang, K.-F. Liu, A. Alexandru, T. Draper, and R. S. Sufian, Lattice Calculation of Nucleon Isovector Axial Charge with Improved Currents, *Phys. Rev. D* **96**, 034519 (2017), arXiv:1612.04388 [hep-lat].
- [36] E. Berkowitz, D. Brantley, C. Bouchard, C. C. Chang, M. A. Clark, N. Garron, B. Joo, T. Kurth, C. Monahan, H. Monge-Camacho, A. Nicholson, K. Orginos, E. Rinaldi, P. Vranas, and A. Walker-Loud, An accurate calculation of the nucleon axial charge with lattice QCD (2017), arXiv:1704.01114 [hep-lat].
- [37] M. F. M. Lutz, U. Sauerwein, and R. G. E. Timmermans, On the axial-vector form factor of the nucleon and chiral symmetry, *Eur. Phys. J. C* **80**, 844 (2020), arXiv:2003.10158 [hep-lat].
- [38] M. S. Mahbub, W. Kamleh, D. B. Leinweber, P. J. Moran, and A. G. Williams (CSSM Lattice), Roper Resonance in 2+1 Flavor QCD, *Phys. Lett. B* **707**, 389 (2012), arXiv:1011.5724 [hep-lat].
- [39] R. G. Edwards, J. J. Dudek, D. G. Richards, and S. J. Wallace, Excited state baryon spectroscopy from lattice QCD, *Phys. Rev. D* **84**, 074508 (2011), arXiv:1104.5152 [hep-ph].
- [40] C. B. Lang and V. Verduci, Scattering in the πN negative parity channel in lattice QCD, *Phys. Rev. D* **87**, 054502 (2013), arXiv:1212.5055 [hep-lat].
- [41] M. S. Mahbub, W. Kamleh, D. B. Leinweber, P. J. Moran, and A. G. Williams, Structure and Flow of the Nucleon Eigenstates in Lattice QCD, *Phys. Rev. D* **87**, 094506 (2013), arXiv:1302.2987 [hep-lat].
- [42] G. P. Engel, C. B. Lang, D. Mohler, and A. Schäfer (BGR), QCD with Two Light Dynamical Chirally Improved Quarks: Baryons, *Phys. Rev. D* **87**, 074504 (2013), arXiv:1301.4318 [hep-lat].
- [43] J. M. M. Hall, A. C. P. Hsu, D. B. Leinweber, A. W. Thomas, and R. D. Young, Finite-volume matrix Hamiltonian model for a $\Delta \rightarrow N\pi$ system, *Phys. Rev. D* **87**, 094510 (2013), arXiv:1303.4157 [hep-lat].
- [44] D. S. Roberts, W. Kamleh, and D. B. Leinweber, Wave Function of the Roper from Lattice QCD, *Phys. Lett. B* **725**, 164 (2013), arXiv:1304.0325 [hep-lat].
- [45] D. S. Roberts, W. Kamleh, and D. B. Leinweber, Nucleon Excited State Wave Functions from Lattice QCD, *Phys. Rev. D* **89**, 074501 (2014), arXiv:1311.6626 [hep-lat].
- [46] C. Alexandrou, T. Leontiou, C. N. Papanicolas, and E. Stiliaris, Novel analysis method for excited states in lattice QCD: The nucleon case, *Phys. Rev. D* **91**, 014506 (2015), arXiv:1411.6765 [hep-lat].
- [47] Z.-W. Liu, W. Kamleh, D. B. Leinweber, F. M. Stokes, A. W. Thomas, and J.-J. Wu, Hamiltonian effective field theory study of the $N^*(1535)$ resonance in lattice QCD, *Phys. Rev. Lett.* **116**, 082004 (2016), arXiv:1512.00140 [hep-lat].
- [48] A. L. Kiratidis, W. Kamleh, D. B. Leinweber, and B. J. Owen, Lattice baryon spectroscopy with multiparticle interpolators, *Phys. Rev. D* **91**, 094509 (2015), arXiv:1501.07667 [hep-lat].
- [49] D. Leinweber, W. Kamleh, A. Kiratidis, Z.-W. Liu, S. Mahbub, D. Roberts, F. Stokes, A. W. Thomas, and J. Wu, N^* Spectroscopy from Lattice QCD: The Roper Explained, *JPS Conf. Proc.* **10**, 010011 (2016), arXiv:1511.09146 [hep-lat].
- [50] F. M. Stokes, W. Kamleh, D. B. Leinweber, M. S. Mahbub, B. J. Menadue, and B. J. Owen, Parity-expanded variational analysis for nonzero momentum, *Phys. Rev. D* **92**, 114506 (2015), arXiv:1302.4152 [hep-lat].
- [51] A. L. Kiratidis, W. Kamleh, D. B. Leinweber, Z.-W. Liu, F. M. Stokes, and A. W. Thomas, Search for low-lying lattice QCD eigenstates in the Roper regime, *Phys. Rev. D* **95**, 074507 (2017), arXiv:1608.03051 [hep-lat].
- [52] Z.-W. Liu, W. Kamleh, D. B. Leinweber, F. M. Stokes, A. W. Thomas, and J.-J. Wu, Hamiltonian effective field theory study of the $N^*(1440)$ resonance in lattice QCD, *Phys. Rev. D* **95**, 034034 (2017), arXiv:1607.04536 [nucl-th].
- [53] J.-J. Wu, H. Kamano, T. S. H. Lee, D. B. Leinweber, and A. W. Thomas, Nucleon resonance structure in the finite volume of lattice QCD, *Phys. Rev. D* **95**, 114507 (2017), arXiv:1611.05970 [hep-lat].
- [54] C. B. Lang, L. Leskovec, M. Padmanath, and S. Prelovsek, Pion-nucleon scattering in the Roper channel from lattice QCD, *Phys. Rev. D* **95**, 014510 (2017), arXiv:1610.01422 [hep-lat].

- [55] J.-j. Wu, D. B. Leinweber, Z.-w. Liu, and A. W. Thomas, Structure of the Roper Resonance from Lattice QCD Constraints, *Phys. Rev. D* **97**, 094509 (2018), arXiv:1703.10715 [nucl-th].
- [56] C. W. Andersen, J. Bulava, B. Hörz, and C. Morningstar, Elastic $I = 3/2p$ -wave nucleon-pion scattering amplitude and the $\Delta(1232)$ resonance from $N_f=2+1$ lattice QCD, *Phys. Rev. D* **97**, 014506 (2018), arXiv:1710.01557 [hep-lat].
- [57] F. M. Stokes, W. Kamleh, and D. B. Leinweber, Elastic Form Factors of Nucleon Excitations in Lattice QCD, *Phys. Rev. D* **102**, 014507 (2020), arXiv:1907.00177 [hep-lat].
- [58] F. M. Stokes, W. Kamleh, and D. B. Leinweber, Structure and transitions of nucleon excitations via parity-expanded variational analysis, *PoS LATTICE2019*, 182 (2019), arXiv:2001.07919 [hep-lat].
- [59] A. Virgili, W. Kamleh, and D. B. Leinweber, Role of chiral symmetry in the nucleon excitation spectrum, *Phys. Rev. D* **101**, 074504 (2020), arXiv:1910.13782 [hep-lat].
- [60] T. Khan, D. Richards, and F. Winter, Positive-parity baryon spectrum and the role of hybrid baryons, *Phys. Rev. D* **104**, 034503 (2021), arXiv:2010.03052 [hep-lat].
- [61] C. Morningstar, J. Bulava, A. D. Hanlon, B. Hörz, D. Mohler, A. Nicholson, S. Skinner, and A. Walker-Loud, Progress on Meson-Baryon Scattering, *PoS LATTICE2021*, 170 (2022), arXiv:2111.07755 [hep-lat].
- [62] C. D. Abell, D. B. Leinweber, A. W. Thomas, and J.-J. Wu, Regularization in nonperturbative extensions of effective field theory, *Phys. Rev. D* **106**, 034506 (2022), arXiv:2110.14113 [hep-lat].
- [63] J. Bulava, A. D. Hanlon, B. Hörz, C. Morningstar, A. Nicholson, F. Romero-López, S. Skinner, P. Vranas, and A. Walker-Loud, Elastic nucleon-pion scattering at $m_\pi=200$ MeV from lattice QCD, *Nucl. Phys. B* **987**, 116105 (2023), arXiv:2208.03867 [hep-lat].
- [64] J. Bulava *et al.*, Low-lying baryon resonances from lattice QCD (2023) arXiv:2310.08375 [hep-lat].
- [65] C. D. Abell, D. B. Leinweber, A. W. Thomas, and J.-J. Wu, Effects of multiple single-particle basis states in scattering systems (2023), arXiv:2305.18790 [nucl-th].
- [66] C. D. Abell, D. B. Leinweber, Z.-W. Liu, A. W. Thomas, and J.-J. Wu, Low-lying odd-parity nucleon resonances as quark-model like states (2023), arXiv:2306.00337 [hep-lat].
- [67] P. Wang and A. W. Thomas, The First Moments of Nucleon Generalized Parton Distributions, *Phys. Rev. D* **81**, 114015 (2010), arXiv:1003.0957 [hep-ph].
- [68] A. Scapellato, C. Alexandrou, K. Cichy, M. Constantinou, K. Hadjiyiannakou, K. Jansen, and F. Steffens, Generalized parton distributions of the proton from lattice QCD, *PoS LATTICE2021*, 129 (2022), arXiv:2111.03226 [hep-lat].
- [69] F. He, C.-R. Ji, W. Melnitchouk, A. W. Thomas, and P. Wang, Generalized parton distributions of sea quarks in the proton from nonlocal chiral effective theory, *Phys. Rev. D* **106**, 054006 (2022), arXiv:2202.00266 [hep-ph].
- [70] H.-W. Lin, Pion valence-quark generalized parton distribution at physical pion mass, *Phys. Lett. B* **846**, 138181 (2023).
- [71] P. M. Copeland, C.-R. Ji, and W. Melnitchouk, Octet and decuplet baryon self-energies in relativistic $su(3)$ chiral effective theory, *Phys. Rev. D* **103**, 094019 (2021).
- [72] E. Jenkins and A. V. Manohar, Chiral corrections to the baryon axial currents, *Physics Letters B* **259**, 353 (1991).
- [73] M. Lutz and E. Kolomeitsev, Relativistic chiral $su(3)$ symmetry, large- nc sum rules and meson-baryon scattering, *Nuclear Physics A* **700**, 193 (2002).
- [74] T. Ledwig, J. M. Camalich, L. S. Geng, and M. J. V. Vacas, Octet-baryon axial-vector charges and $su(3)$ -breaking effects in the semileptonic hyperon decays, *Phys. Rev. D* **90**, 054502 (2014).
- [75] J. A. Oller, M. Verbeni, and J. Prades, Meson-baryon effective chiral lagrangians to $\mathcal{O}(q^3)$, *Journal of High Energy Physics* **2006**, 079 (2006).
- [76] J. Gasser, M. Sainio, and A. Švarc, Nucleons with chiral loops, *Nuclear Physics B* **307**, 779 (1988).
- [77] N. Fettes, U.-G. Meißner, M. Mojžiš, and S. Steininger, The chiral effective pion-nucleon lagrangian of order p_4 , *Annals of Physics* **283**, 273 (2000).
- [78] T. Fuchs, J. Gegelia, G. Japaridze, and S. Scherer, Renormalization of relativistic baryon chiral perturbation theory and power counting, *Phys. Rev. D* **68**, 056005 (2003).
- [79] D. S. Armstrong and R. D. McKeown, Parity-Violating Electron Scattering and the Electric and Magnetic Strange Form Factors of the Nucleon, *Ann. Rev. Nucl. Part. Sci.* **62**, 337 (2012), arXiv:1207.5238 [nucl-ex].
- [80] K. A. Aniol *et al.* (HAPPEX), Measurement of the neutral weak form-factors of the proton, *Phys. Rev. Lett.* **82**, 1096 (1999), arXiv:nucl-ex/9810012.
- [81] D. Androic *et al.* (G0), Strange Quark Contributions to Parity-Violating Asymmetries in the Backward Angle G0 Electron Scattering Experiment, *Phys. Rev. Lett.* **104**, 012001 (2010), arXiv:0909.5107 [nucl-ex].
- [82] A. W. Thomas, A Limit on the Pionic Component of the Nucleon Through $SU(3)$ Flavor Breaking in the Sea, *Phys. Lett. B* **126**, 97 (1983).
- [83] A. W. Thomas, Chiral Symmetry and the Bag Model: A New Starting Point for Nuclear Physics, *Adv. Nucl. Phys.* **13**, 1 (1984).
- [84] A. W. Thomas, Chiral extrapolation of hadronic observables, *Nucl. Phys. B Proc. Suppl.* **119**, 50 (2003), arXiv:hep-lat/0208023.
- [85] J. F. Donoghue, B. R. Holstein, and B. Borasoy, $SU(3)$ baryon chiral perturbation theory and long distance regularization, *Phys. Rev. D* **59**, 036002 (1999), arXiv:hep-ph/9804281.
- [86] J. M. M. Hall, F. X. Lee, D. B. Leinweber, K. F. Liu, N. Mathur, R. D. Young, and J. B. Zhang, Chiral extrapolation beyond the power-counting regime, *Phys. Rev. D* **84**, 114011 (2011), arXiv:1101.4411 [hep-lat].
- [87] J. A. McGovern and M. C. Birse, Convergence of the chiral expansion for the nucleon mass, *Phys. Rev. D* **74**, 097501 (2006), arXiv:hep-lat/0608002.
- [88] J. M. Alarcon, J. Martin Camalich, J. A. Oller, and L. Alvarez-Ruso, πN scattering in relativistic baryon chiral perturbation theory revisited, *Phys. Rev. C* **83**, 055205 (2011), [Erratum: *Phys.Rev.C* 87, 059901 (2013)], arXiv:1102.1537 [nucl-th].
- [89] M. Frink, U.-G. Meißner, and I. Scheller, Baryon masses, chiral extrapolations, and all that, *Eur. Phys. J. A* **24**, 395 (2005), arXiv:hep-lat/0501024.
- [90] D. Djukanovic, M. R. Schindler, J. Gegelia, and S. Scherer, Improving the ultraviolet behavior in baryon chiral perturbation theory, *Phys. Rev. D* **72**, 045002 (2005).

- [91] M. Frink and U.-G. Meißner, Chiral extrapolations of baryon masses for unquenched three-flavor lattice simulations, *Journal of High Energy Physics* **2004**, 028 (2004).
- [92] D. Siemens, J. R. de Elvira, E. Epelbaum, M. Hoferichter, H. Krebs, B. Kubis, and U.-G. Meißner, Reconciling threshold and subthreshold expansions for pion–nucleon scattering, *Physics Letters B* **770**, 27 (2017).
- [93] B. J. Menadue, W. Kamleh, D. B. Leinweber, and M. S. Mahbub, Isolating the $\Lambda(1405)$ in Lattice QCD, *Phys. Rev. Lett.* **108**, 112001 (2012), arXiv:1109.6716 [hep-lat].
- [94] M. Lüscher, Properties and uses of the wilson flow in lattice QCD, *Journal of High Energy Physics* **2010**, 71 (2010).
- [95] S. Steininger, U.-G. Meißner, and N. Fettes, On wave function renormalization and related aspects in heavy fermion effective field theories, *Journal of High Energy Physics* **1998**, 008 (1998).
- [96] T. Becher and H. Leutwyler, Baryon chiral perturbation theory in manifestly lorentz invariant form, *The European Physical Journal C - Particles and Fields* **9**, 643 (1999).
- [97] M. R. Schindler, D. Djukanovic, J. Gegelia, and S. Scherer, Chiral expansion of the nucleon mass to order $\mathcal{O}(q^6)$, *Physics Letters B* **649**, 390 (2007).
- [98] M. Hoferichter, J. Ruiz de Elvira, B. Kubis, and U.-G. Meißner, On the role of isospin violation in the pion–nucleon σ -term, *Physics Letters B* **843**, 138001 (2023).
- [99] J. Ruiz de Elvira, M. Hoferichter, B. Kubis, and U.-G. Meißner, Extracting the σ -term from low-energy pion-nucleon scattering, *J. Phys. G* **45**, 024001 (2018), arXiv:1706.01465 [hep-ph].
- [100] J. M. Alarcón, J. M. Camalich, and J. A. Oller, Chiral representation of the πN scattering amplitude and the pion-nucleon sigma term, *Phys. Rev. D* **85**, 051503 (2012).
- [101] Y.-B. Yang, A. Alexandru, T. Draper, J. Liang, and K.-F. Liu (xQCD), πN and strangeness sigma terms at the physical point with chiral fermions, *Phys. Rev. D* **94**, 054503 (2016), arXiv:1511.09089 [hep-lat].
- [102] C. Alexandrou, S. Bacchio, M. Constantinou, J. Finkenrath, K. Hadjiyiannakou, K. Jansen, G. Koutsou, and A. Vaquero Aviles-Casco, Nucleon axial, tensor, and scalar charges and σ -terms in lattice QCD, *Phys. Rev. D* **102**, 054517 (2020), arXiv:1909.00485 [hep-lat].
- [103] T. E. O. Ericson, A New Interpretation of the $\pi N \sigma$ - Term, *Phys. Lett. B* **195**, 116 (1987).
- [104] S. Scherer and M. R. Schindler, *A primer for chiral perturbation theory*, Vol. 830 (Springer Science & Business Media, 2011).